Phosphate assisted integrated carbon dioxide capture and conversion to methane

Christopher J Koch, Anushan Alagaratnam, Alain Goeppert, G.K. Surya Prakash*

Phosphate salts have been previously studied as carbon dioxide capture reagents. However, the direct conversion of the captured carbon dioxide species to hydrogenated products is not well studied with phosphate-assisted systems. Herein, we report the conversion of captured carbon dioxide to methane in such a system. When a nickel-based catalyst was used, the reactivity was strongly inhibited due to unwanted interaction of nickel with the phosphate species present in the system. However, with $5\%Ru/Al_2O_3$ as the catalyst, 100% conversion of captured CO_2 to methane was achieved after 6 hours under 50 bar H_2 at 200 °C. $5\%Ru/Al_2O_3$ ¬was also able to maintain its reactivity over several capture/hydrogenation cycles.

DOI: 10.1039/d3se00390f

Introduction

Rising carbon dioxide levels in the atmosphere are a growing concern as they contribute to several environmental issues associated with global warming. Thus, it is important to find ways to reduce the anthropogenic carbon emissions with the use of technologies such as solar and wind energy wherever possible. In other cases and for hard to decarbonize sectors, CO₂ capture and sequestration or utilization will be needed. CO₂ can be captured either at the source of emission or from the atmosphere.^{1–4} One way of accomplishing this is by capturing carbon dioxide using simple chemical reagents, usually acting as bases. For instance, amines (e.g. mono- and di-ethanol amines) and hydroxide salts (e.g. NaOH) are often used as capture materials.^{5–12} Both of these capture materials have their own merits and drawbacks when it comes to uses in industrial settings. Amines and polyamines allow for flexible organic scaffolds to be embedded in the material to tailor and improve the performance, but there are often associated with volatility and stability issues.^{13–17} Hydroxide salts do not have these volatility concerns but capture carbon dioxide in the form of carbonate/bicarbonate salts that generally require very high temperatures to liberate the captured CO₂ and regenerate the hydroxide salt.^{18,19}

While a vast literature exists for the capture of CO_2 with amines and hydroxide salts, the number of reports on phosphate salts being used for CO_2 capture are scarce. Only a handful of studies on trisodium phosphate (Na_3PO_4) and other phosphates and their utilization as carbon dioxide capture agents either by themselves or in mixtures with amines could be identified. Phosphate salts were proposed for CO_2 capture hoping that they would release the captured CO_2 at lower temperatures than hydroxide-based systems while not experiencing the volatility and stability concerns that are associated with amines. Although potassium and sodium phosphate salts are soluble in water, they often have a more limited selection of other solvents in which they are soluble in and have lower solubility compared to capture agents like amines and hydroxide salts. The solvent scope is of particular importance when considering a capture media from a carbon capture and utilization approach (CCU) to an integrated

carbon capture and conversion system (ICCC). While ICCC routes are being increasingly explored as a possible way to save energy and simplify/intensify the capture and utilization of CO₂, many of these systems are utilizing homogenous catalysts that can operate in organic solvents such as ethylene glycol but have performance issues in aqueous solutions.^{6,8,10} To date, ICCC technologies have not been extensively studied with heterogeneous catalysts.^{9,11} Exploring that route could open up other pathways enabling the use of other capture reagents like phosphate salts, that are difficult to utilize in association with homogenous catalysts.

Heterogenous catalysts based on metals like ruthenium and nickel often serve as methanation catalysts when a gas stream of CO₂ is used as the reagent in the well-known Sabatier process.^{26,27} These flow reactions are routinely performed at relatively low pressures, but at higher reaction temperatures of 300-400 °C or above. There are reports on utilizing heterogenous catalysts in capture and conversion technologies.^{28–30} However, these processes usually use bifunctional solid materials combining an alkali or alkaline earth metal mixed with the catalyst to capture and convert CO2 in two consecutive steps. In a first step the alkali or alkaline earth metal species on the surface reacts with CO2 to form carbonate/bicarbonate salts. In a second step these salts are decomposed to form CO₂ which is then hydrogenated to methane over the embedded catalyst at temperatures generally above 500 °C.31-33 Because the catalyst and the adsorbent are intimately associated in the same solid, a large amount of catalyst is tied up in the material and unused during the adsorption phase, which can be capital intensive. This also means that the catalytic component of the bifunctional material can be oxidized or deactivated during the adsorption phase when exposed to atmospheric and industrial gas flows. During the hydrogenation phase the catalyst would then have to be reduced again in each consecutive CO2 capture/hydrogenation cycle. Having the ability to separate the capturing agent from the catalyst would thus be advantageous, allow for more flexibility in the process design, and lower the amount of catalyst needed.

Herein, we report such a system in which carbon dioxide is first captured with a phosphate salt. In a second, separate step, the carbonate/bicarbonate species formed with this capturing agent are converted to methane. This conversion occurs at relatively mild temperatures of 150 to 200 °C and can be completed successfully in six hours over a $5\%Ru/Al_2O_3$ catalyst.

Results and Discussion

Trisodium phosphate dodecahydrate, $Na_3PO_4\cdot 12H_2O$, reacts in aqueous solution with carbon dioxide to form disodium hydrogen phosphate and sodium bicarbonate (Eq. 1).

Prakash et al. has recently shown that both sodium carbonate, sodium bicarbonate as well as other alkali metal carbonates in aqueous solution could be hydrogenated to methane using a nickel-based catalyst (25%Ni/Al₂O₃).³⁴ Following this report, the same catalyst was initially used to test the conversion of carbon dioxide captured with trisodium phosphate to methane at 200 °C under a hydrogen pressure of 50 bar. This experiment led to a poor methane yield of only 2.6% in 6 hours (Table 1), which was likely the result of phosphorous compounds acting as ligand and binding to the nickel-based catalyst, inhibiting its reactivity (Figure S16 displaying the XRD of 25% Ni/Al₂O₃ after reaction and

showing Ni-P containing species). It has previously been reported that phosphorous in phosphorous containing compounds can poison nickel catalyst in the hydrogenation reactions over Raney Nickel and Lindlar's Pd catalysts.35-37 In electrochemical systems, where nickel is the active species in phosphate buffered systems, an additive can be used as a sacrificial metal. For example, zinc metal is sometimes employed as a sink so that phosphorous will bind with zinc rather than with the active metal, allowing for the reactivity of the active metal to be retained. 38-40 In an attempt to prevent phosphorous compounds from binding nickel, zinc was therefore added to the catalyst (12%Ni/3%Zn/Al₂O₃). Unfortunately, zinc did not prohibit the binding of phosphorous to nickel and led to a similar outcome (shown in Figure S17), resulting in a 1.4% methane yield in 6 hours. This could be due to the excess of phosphate in comparison to the amount of nickel and zinc present on the catalyst. As utilizing nickel as the active metal did not seem to be compatible with the use of phosphates, another catalyst based on the ruthenium metal was tested. Ruthenium-based heterogenous catalyst have also been reported to form phosphorous poisoned sites when reacted with phosphate salts but under harsher conditions, specifically above temperatures of 400 °C (and can be seen in Figure S18). 41–43 When 5%Ru/Al₂O₃ was used, the conversion of captured carbon dioxide to methane was quantitative in six hours at 200 °C. This shows that phosphate-assisted capture systems could be used in an integrated capture and conversion process to produce methane under our reaction conditions. The catalysts were characterized by powder X-ray diffraction (XRD), Scanning electron microscopy (SEM), and X-ray fluorescence (XRF) and the results can be found in the SI.

Table 1. Catalyst screening for the hydrogenation of the reaction product of Na₃PO₄ and CO₂

Catalyst	Captured CO ₂	Methane produced	Methane yield (%)	Methane productivity
	(mmol)	(mmol)		(g _{methane} ·h ⁻ ¹·kg _{cat} -¹)
25%Ni/	7.1	0.2	2.55	1.61
Al ₂ O ₃				
12%Ni/ 3%Zn/	7.1	0.1	1.44	0.90
Al ₂ O ₃				
5%Ru/	7.1	7.1	100	63.3
Al_2O_3				

Conditions: 10 mmol Na_3PO_4 after 3 hours under pure CO_2 stream, 10 mL DI H2O, 200 °C, 6 hours reaction time, 300 mg catalyst, 50 bar H_2 . Yields calculated by gas chromatography are within $\pm 5\%$.

After determining that 5%Ru/Al₂O₃ was a suitable catalyst for this reaction, other reaction parameters were optimized as shown in Table 2. All experiments used 10 mmol of sodium phosphate tribasic in 10 mL of distilled water as the capture material and after three hours under a pure CO₂ stream, 7.1 mmol of CO₂ was captured per 10 mmol of sodium phosphate employed. In the hydrogenation reaction following the capture, decreasing the reaction time from 6 hours to 3 hours resulted in a substantial decrease in methane yield from 100% to 58.9%. Upon decreasing the reaction time further to 1 hour the methane yield was only 28.2%. Consequently, 6 hour optimal reaction time was used for the rest of the study. The catalyst morphology obtained by SEM imaging before and after the reaction (conditions: 10 mmol Na₃PO₄ after 3 hours under pure CO₂ stream, 10 mL DI H₂O, 200 °C, 6 hours reaction time, 300 mg 5%Ru/Al₂O₃, 50 bar H₂) is shown in Figure S20 and S21, respectively.

Table 2. Screening of reaction parameters for the hydrogenation reaction catalyzed by 5%Ru/Al₂O₃

Captured CO ₂ (mmol)	5%Ru/Al ₂ O ₃ (mg)	Temperature (°C)	Time (hour)	H ₂ pressure (bar)	Methane produced (mmol)	Methane yield (%)	Methane productivity (g _{methane} ·h ⁻ 1·kg _{cat} ⁻¹)
7.1	300	200	6	50	7.1	100	63.3
7.1	300	200	3	50	4.2	58.9	74.6
7.1	300	200	1	50	2.0	28.2	107.2
7.1	300	200	6	40	6.3	88.7	56.1
7.1	300	200	6	30	3.9	54.3	34.3
7.1	300	170	6	50	5.1	71.9	45.5
7.1	300	150	6	50	3.9	54.2	34.3
7.1	150	200	6	50	4.7	66.7	84.4
7.1	50	200	6	50	3.6	47.3	179.4
11.3 ^[a]	300	200	6	50	7.3	64.2	65.1
11.3 ^[a]	300	200	6	60	9.5	84.1	84.7

Conditions: 10 mmol Na_3PO_4 after 3 hours under pure CO_2 stream, 10 mL DI H_2O , 200 °C. [a] Na_3PO_4 was under a CO_2 stream for 12 hours. Yields calculated by gas from Gas chromatography are within $\pm 5\%$.

At first, the pressure was varied. A pressure of 50 bar of H_2 (pressure at room temperature when filing the reactor) resulted in a 100% yield. Decreasing the pressure to 40 bar lowered somewhat the yield to 88.7%. Further decreasing the hydrogen pressure to 30 bar resulted in a yield of only 54.3%. Thus, 50 bar was selected as the preferred pressure for the rest of the optimization.

Reaction temperature also played an important role in the catalysis. Decreasing the temperature from 200 °C to 170 °C resulted in a decrease in methane yield from 100% to 71.9%. Upon further decreasing the temperature to 150 °C the methane yield was only 54.7%. The latter temperature, 150 °C is similar to reaction conditions reported for integrated capture and conversion to methanol process using homogenous catalysis so it is interesting note that that the catalytic methanation reaction was still taking place at these lower temperatures. $^{6.7,44,45}$

Catalyst loading was varied as well. As expected, the yield decreased with less catalyst present in the system. When 300 mg of catalyst was used methane was obtained in a 100% yield and a productivity of 63.3 gmethane·h-1·kgcat-1. At a catalyst loading of 150 and 50 mg, the methane yield decreased to 66.7% and 47.3%, respectively. However, the methane productivity increased. When 150 mg of catalyst was used a methane productivity of 84.4 gmethane·h-1·kgcat-1 was obtained. Further decreasing the amount of catalyst to 50 mg resulted in a methane productivity of 179.4 gmethane·h-1·kgcat-1. Thus, lower loadings seemed to lead to a more efficient use of the catalyst.

Increasing the time of the capture from 3 hours to 12 hours led to an increase in the CO_2 captured from 7.3 mmol CO2 to 11.3 mmol. CO2 capture over 3 hours led to a mixture of sodium phosphate dibasic and tribasic was obtained as shown in the 31P NMR spectrum of the capture solution

(Figure S7). Over 12 h of capture, the solution contained mostly sodium phosphate dibasic (31P NMR, Figure S8). Utilizing the optimized conditions of 300 mg 5%Ru/Al₂O₃, 50 bar H₂, 6 hours of reaction time, and 200 °C resulted in a 64.2% yield and 7.3 mmol of methane being produced. When the reaction pressure was increased from 50 bar H2 to 60 bar H2, 9.5 mmol of methane was produced, resulting in a yield of 84.1%.

Additional phosphate salts were tested for both their ability to capture carbon dioxide and also for subsequent conversion to methane as shown in Table 3. All capture experiments were conducted over 3 hours under a pure CO₂ stream. Both sodium and potassium phosphate salts were able to undergo conversion as well. 10 mmol of potassium phosphate captured 11.3 mmol CO2 in 3 hours. This was more than the 7.1 mmol CO2 captured with sodium phosphate over the same period. However, over the six-hour hydrogenation time only 7.3 mmol of the captured CO₂ was converted to methane. This result is similar to the one obtained with sodium phosphate when the capture time was 12 hours instead of 3, where 11.3 mmol of CO₂ was captured but only 7.3 mmol was converted to methane. Calcium and lithium phosphate were also tested. However, the amount of CO₂ that calcium phosphate captured was significantly lower, at 1.6 mmol CO₂. Of the 1.6 mmol captured, only 0.48 mmol was converted to methane. Lithium phosphate also was not efficient in capturing CO2 with only 0.63 mmol of CO₂ captured in three hours under a CO2 stream. Of the 0.63 mmol CO₂ captured only 0.18 was converted to methane. Calcium and lithium phosphate most likely performed worse than sodium and potassium due to their lower solubility in water. 46,47

Table 3. Screening of phosphate salts for the capture/hydrogenation of CO₂

Phosphate	CO_2	Methane	Methane
	captured	produced	yield
		(mmol)	(%)[a]
Li ₃ PO ₄	0.63	0.21	33.3
Na ₃ PO ₄	7.1	7.1	100
K_3PO_4	11.3	7.3	64.6
$Ca_3(PO_4)_2$	1.63	0.48	29.4

Conditions: 10 mmol phosphate salt after 3 hours under pure CO_2 stream, 10 mL DI H2O, 200 °C, 6 hours reaction time, 300 mg 5%Ru/Al₂O₃, 50 bar H₂. Yields calculated by gas chromatography are within ±5%. [a] based on the amount of CO_2 captured.

The recyclability of both the catalyst and the phosphate salt was then tested. For the recycling experiments sodium phosphate solution was utilized and before each cycle was placed under a pure CO_2 stream for three hours. The capture media was then placed in a reactor with the catalyst. After the reaction the media was separated from the catalyst to be used for the subsequent CO_2 capture and the catalyst was stored in an inert atmosphere until the next cycle was conducted. The first three cycles were performed without any noticeable deactivation in the catalyst or the base. However, upon continuing to the fourth cycle a significant deactivation of the base was observed. After the third cycle of reactivity, only 2.6 mmol of CO_2 was captured, which was a significant decrease from the 7.1 mmol captured in the previous three cycles. In the fifth cycle the amount of CO_2 captured decreased further to 2 mmol. The catalyst, on the other hand, was still able to perform quantitative conversions of the captured CO_2 to methane over fourth and fifth cycle. It was noticed that the crystallite size of the $SCRU/Al_2O_3$ catalyst remained relatively consistent over the five cycles. The crystallite size of the ruthenium metal was 217 Å before the reaction and 224 Å after five cycles (Table S1 showing the

crystallite size obtained by XRD). This indicates that a deactivation of the base seems to occur over the course of the recycling experiments.

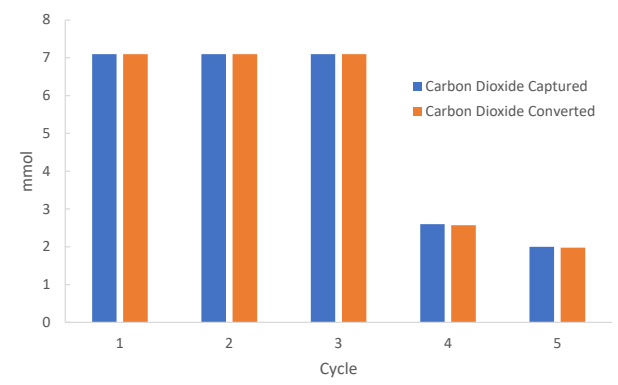


Figure 1. CO₂ capture with Na₃PO₄ and hydrogenation to methane on 5%Ru/Al₂O₃ over 5 consecutive cycles.

In order to understand the observed deactivation, the solid phase of the reaction mixture after 5 consecutive capture/hydrogenation cycles with Na3PO4 was analyzed by X-Ray diffraction. This solid phase obtained by decantation contained both the ruthenium catalyst and some white solid that had formed in the reaction and was insoluble in water. The X-Ray diffraction pattern of this solid mixture shown in Figure S19 revealed the formation of aluminum phosphate AIPO₄ that was the result of the reaction of phosphate species with the alumina catalyst support over several capture/hydrogenation cycles. Previously it had been reported that aluminum phosphate could be synthesized with phosphoric acid and alumina, often using elevated temperatures of 250 °C.^{48–50} Dibasic and monobasic sodium phosphate have both also been previously reported for the synthesis of AIPO₄. ⁵¹ However, there are not many reports of tribasic sodium phosphate being utilized for the synthesis of AIPO₄. In Figures S10 and S11, it was observed by 31P NMR that after several cycles, phosphate salts present in the solution shifted to more acidic species, i.e. from tribasic to dibasic and mixtures with monobasic sodium phosphate. As the solution became more acidic it was more likely able to interact with the alumina to form AIPO₄. This relatively slow and progressive transformation could explain why quantitative recycling was still observed in the first three cycles, and a large loss in the capture capacity was only noticed after the third cycle as the capture agent became depleted through the formation of AIPO4. The shift to more acidic species could also have led to lower level of CO2 capture as these species have much less affinity for CO₂.

The XRD spectrum of the solid containing the catalyst after the hydrogenation reaction (Figure S18 and S19) also revealed the presence of peaks that can be assigned to ruthenium phosphide (RuP₂). RuP2 has been obtained in previous studies even at temperatures as low as $60\,^{\circ}\text{C}$. This could lead to some of the phosphate salt in the system to be used up over the course of the reaction; however, given the low concentration of ruthenium in the catalyst, this pathway is much more limited compared to the formation of AlPO₄.

Conclusion

We have shown the possibility to convert carbon dioxide to methane using an aqueous phosphate mediated capture system. Previously, limited solubility the phosphate salts in organic solvents had restricted their applications in direct capture and conversion processes as many of them utilize organic solvents. Utilizing nickel led to catalyst deactivation as phosphorous binding was too strong and inhibited further reactivity. However, using water and a 5%Ru/Al2O3 catalyst, quantitative conversions of captured CO₂ to methane was obtained within six hours. The system was also able to undergo several cycles of CO₂ capture/hydrogenation but showed signs of deactivation of the base after the third cycle. Nevertheless, the catalyst maintained a high reactivity throughout each cycle and showed near quantitative conversion even after the base deactivated and inhibited further CO₂ capture.

Acknowledgment

Support of our work by the Loker Hydrocarbon Research Institute at the University of Southern California is gratefully acknowledged. We would like to thank the National Science Foundation (award: CHE-2018740) for the purchase of the diffractometer used to obtain powder diffraction patterns reported here. We would also like to thank the Center of Excellence for Nano Imaging (CNI) at the University of Southern California for microscope time and access to the XRF.

Conflicts of interest

The authors report no conflicts of interest.

Author Contributions

Corresponding Author:* gprakash@usc.edu

ORCID:

Christopher J Koch: 0000-0003-0565-6853

Anushan Alagaratnam: 0000-0002-9339-7814

Alain Goeppert: 0000-0001-8667-8530

G. K. Surya Prakash: 0000-0002-6350-8325

References

- 1 S. Kammerer, I. Borho, J. Jung and M. S. Schmidt, Int J Environ Sci Technol, 2022.
- 2 X. Wang and C. Song, Front Energy Res, 2020, 8.
- A. Goeppert, M. Czaun, G. K. Surya Prakash and G. A. Olah, Energy Environ Sci, 2012, 5, 7833–7853.
- 4 E. S. Sanz-Pérez, C. R. Murdock, S. A. Didas and C. W. Jones, Chem Rev, 2016, 116, 11840–11876.

- 5 B. Li, Y. Duan, D. Luebke and B. Morreale, Appl Energy, 2013, 102, 1439–1447.
- 6 R. Sen, A. Goeppert and G. K. S. Prakash, J Organomet Chem, 2022, 965–966, 122331.
- 7 R. Sen, A. Goeppert, S. Kar and G. K. S. Prakash, J Am Chem Soc, 2020, 142, 4544–4549.
- 8 R. Sen, C. J. Koch, A. Goeppert and G. K. S. Prakash, ChemSusChem, 2020, 13, 6318–6322.
- 9 J. Kothandaraman and D. J. Heldebrant, Green Chem., 2020, 22, 828–834.
- 10 S. Kar, J. Kothandaraman, A. Goeppert and G. K. S. Prakash, J CO2 Util, 2018, 23, 212–218.
- J. Kothandaraman, J. S. Lopez, Y. Jiang, E. D. Walter, S. D. Burton, R. A. Dagle and D. J. Heldebrant, Adv Energy Mater, 2022, 12, 2202369.
- S. Kar, R. Sen, J. Kothandaraman, A. Goeppert, R. Chowdhury, S. B. Munoz, R. Haiges and G. K. S. Prakash, J Am Chem Soc, 2019, 141, 3160–3170.
- 13 M. Jahandar Lashaki, S. Khiavi and A. Sayari, Chem. Soc. Rev., 2019, 48, 3320–3405.
- F. Vega, A. Sanna, B. Navarrete, M. M. Maroto-Valer and V. J. Cortés, Greenh. Gases: Sci Technol, 2014, 4, 707–733.
- 15 Y. Du, Y. Yuan and G. T. Rochelle, Int J Greenh Gas Control, 2017, 58, 1–9.
- 16 S. B. Fredriksen and K.-J. Jens, Energy Procedia, 2013, 37, 1770–1777.
- 17 A. Goeppert, H. Zhang, R. Sen, H. Dang and G. K. S. Prakash, ChemSusChem, 2019, 12, 1712–1723.
- 18 M. Mahmoudkhani and D. W. Keith, Int J Greenh Gas Control, 2009, 3, 376–384.
- 19 I. Ghiat and T. Al-Ansari, J CO2 Util, 2021, 45, 101432.
- 20 R. Radhakrishan, D. M. Do, S. Jaenicke, Y. Sasson and G.-K. Chuah, ACS Catal, 2011, 1, 1631–1636.
- F. S. Souza, M. J. S. Matos, B. R. L. Galvão, A. F. C. Arapiraca, S. N. da Silva and I. P. Pinheiro, Chem Phys Lett, 2019, 714, 143–148.
- 22 M. K. Mondal, J. Singh and D. Khatri, J Chem Eng Data, 2014, 59, 1175–1180.
- 23 T. Sakpal, A. Kumar, Z. M. Aman and R. Kumar, Energies, 2019, 2019, 12, 2889.
- 24 H. K. Balsora and M. K. Mondal, Fluid Phase Equilib, 2012, 328, 21–24.
- 25 H. K. Balsora and M. K. Mondal, J Chem Eng Data, 2011, 56, 4691–4695.
- 26 C. J. Koch, A. Alagaratnam, A. Goeppert and G. K. Surya Prakash, Isr J Chem, 2023, DOI:10.1002/ijch.202200119.
- J. Kothandaraman, J. Saavedra Lopez, Y. Jiang, E. D. Walter, S. D. Burton, R. A. Dagle and D. J. Heldebrant, ChemSusChem, 2021, 14, 4812–4819.

- J. A. Onrubia-Calvo, A. Bermejo-López, S. Pérez-Vázquez, B. Pereda-Ayo, J. A. González-Marcos and J. R. González-Velasco, Fuel, 2022, 320, 123842.
- 29 G. Wang, Y. Guo, J. Yu, F. Liu, J. Sun, X. Wang, T. Wang and C. Zhao, Chem Eng J, 2022, 428, 132110.
- 30 S. J. Park, M. P. Bukhovko and C. W. Jones, Chem Eng J, 2021, 420, 130369.
- A. Dal Pozzo, A. Armutlulu, M. Rekhtina, P. M. Abdala and C. R. Müller, ACS Appl Energy Mater, 2019, 2, 1295–1307.
- D. Jagadeesan, M. Eswaramoorthy and C. N. R. Rao, ChemSusChem, 2009, 2, 878–882.
- 33 S. Lux, G. Baldauf-Sommerbauer and M. Siebenhofer, ChemSusChem, 2018, 11, 3357–3375.
- 34 C. J. Koch, V. Galvan, A. Goeppert and G. K. Surya Prakash, Green Chem., 2023, 25, 1803-1808.
- S. Carenco, A. Leyva-Pérez, P. Concepción, C. Boissière, N. Mézailles, C. Sanchez and A. Corma, Nano Today, 2012, 7, 21–28.
- 36 S. V. L. Mahlaba, A. S. Mahomed and H. B. Friedrich, Appl Catal A Gen, 2018, 565, 163–169.
- D. Albani, K. Karajovic, B. Tata, Q. Li, S. Mitchell, N. López and J. Pérez-Ramírez, ChemCatChem, 2019, 11, 457–464.
- 38 N. Kr. Prasad, A. S. Pathak, S. Kundu and K. Mondal, J Electrochem Soc, 2021, 168, 111504.
- D. G. Yakhvarov, Yu. H. Budnikova, D. I. Tazeev and O. G. Sinyashin, Russ Chem Bull, 2002, 51, 2059–2064.
- 40 N. Kr. Prasad, A. S. Pathak, S. Kundu and K. Mondal, Corros Sci, 2021, 189, 109616.
- T. Fovanna, S. Campisi, A. Villa, A. Kambolis, G. Peng, D. Rentsch, O. Kröcher, M. Nachtegaal and D. Ferri, RSC Adv., 2020, 10, 11507–11516.
- 42 J. Yu, G. Li, H. Liu, L. Zhao, A. Wang, Z. Liu, H. Li, H. Liu, Y. Hu and W. Zhou, Adv Funct Mater, 2019, 29, 1901154.
- H. Ishikawa, S. Yamaguchi, A. Nakata, K. Nakajima, S. Yamazoe, J. Yamasaki, T. Mizugaki and T. Mitsudome, JACS Au, 2022, 2, 419–427.
- J. R. Khusnutdinova, J. A. Garg and D. Milstein, ACS Catal, 2015, 5, 2416–2422.
- 45 R. Sen, C. J. Koch, A. Goeppert and G. K. S. Prakash, ChemSusChem, 2020, 13, 6318-6322.
- D. Mendieta–George, R. Pérez–Garibay, R. Solís–Rodríguez, J. C. Fuentes–Aceituno and A. Alvarado–Gómez, Miner Eng, 2022, 185, 107713.
- 47 K. K. Makinen and E. Soderling, Calcif Tissue Int, 36, 64-71.
- 48 K. Byrappa, J. Shashidhara Prasad and S. Srikantaswamy, J Crystal Growth, 79, 232-235.
- 49 F. Lagno and G. P. Demopoulos, Ind Eng Chem Res, 2005, 44, 8033–8038.

- 50 M. Sh. Khalil, A. A. Hanna and M. A. El-Sayed, Phosphorus Res Bull, 2001, 12, 77–89.
- 51 A. S. Wagh, S. Grover and S. Y. Jeong, J Am Ceram Soc, 2003, 86, 1845–1849.
- 52 Q. Guan, C. Sun, R. Li and W. Li, Catal Commun, 2011, 14, 114–117.
- 53 Q. Chang, J. Ma, Y. Zhu, Z. Li, D. Xu, X. Duan, W. Peng, Y. Li, G. Zhang, F. Zhang and X. Fan, ACS Sustain Chem Eng, 2018, 6, 6388–6394.
- 54 H. Teller, O. Krichevski, M. Gur, A. Gedanken and A. Schechter, ACS Catal, 2015, 5, 4260–4267.
- 55 Q. Wang, Z. Wang, X. Yin, L. Zhou and M. Zhang, Mater Res Bull, 2016, 74, 98–102.
- T. Liu, J. Wang, C. Zhong, S. Lu, W. Yang, J. Liu, W. Hu and C. M. Li, Chemistry A European Journal, 2019, 25, 7826–7830.

Supporting information

Phosphate assisted integrated carbon dioxide capture and conversion to methane

Christopher J. Koch, Anushan Alagaratnam, Alain Goeppert, G.K. Surya Prakash*

Contents

1.	Experimental	12
	1.1 Materials and Methods	12
	1.2 Catalyst Synthesis	12
	1.3 Capture Conditions from Pure CO ₂	12
	1.4 Hydrogenation Conditions	12
	1.5 Recycling Experiments	13
	1.6 Powder X-Ray Diffraction (XRD)	13
	1.7 Scanning Electron Microscopy (SEM)	13
	1.8 X-Ray Fluorescence (XRF)	13
2.	Data	14
	2.1 Gas Chromatography Analysis	14
	2.2 NMR Data	17
	2.3 X-Ray Diffraction Data	25
	2.4 SEM Images	29
	2.5 X-Ray Fluorescence Data (XRF)	30

1. Experimental

1.1 Materials and Methods

All experiments were carried out under an inert atmosphere (with N_2 or Ar) using standard Schlenk techniques. A commercial $5\%Ru/Al_2O_3$ catalyst purchased from Alfa Aesar and was used without further activation or purification. Nickel nitrate hexahydrate (Ni(NO₃)₂·6H₂O) and zinc nitrate hexahydrate (Zn(NO₃)₂·6H₂O) (both 99.9% purity) were purchased from Alfa Aesar. Fumed alumina, Al₂O₃ (Aeroxide AluC) was obtained from Evonik. Potassium (Sigma Aldrich, \geq 98%), sodium (Alfa, \geq 97%), lithium (GFS Chemicals, \geq 98%), and calcium (Thermo Scientific, \geq 98%) phosphate were used without further purification. D₂O (CIL, D-99.9%), toluene-d₈ (CIL, D-99.9%) and imidazole (Fischer, 99.5%) were used as received. ³¹P and ¹³C NMR spectra were recorded on 400, 500 or 600 MHz, Varian NMR spectrometers. ¹³C NMR chemical shifts were determined relative to the residual solvent signals. ³¹P NMR were reference to an internal standard, triphenylphosphine oxide (Sigma Aldrich, 98%). The gas mixtures were analyzed using a Thermo Finnigan gas chromatograph (column: Supelco, Carboxen 1010 plot, 30 m X 0.53 mm) equipped with a TCD detector (CO detection limit: 0.099 v/v%). CO₂ (Gilmore, instrument grade), H₂ (Gilmore, ultra-high pure grade 5.0), Methane (Gilmore, instrument grade).

1.2 Catalyst Synthesis

The $25\% Ni/Al_2O_3$ and the $12\% Ni/3\% Zn/Al_2O_3$ catalysts were synthesized in the following way. A known amount of nickel nitrate hexahydrate (Ni(NO₃)₂·6H₂O) and zinc nitrate hexahydrate (Ni(NO₃)₂·6H₂O) were dissolved into 100 mL of DI water to either synthesize the $25\% Ni/Al_2O_3$ or the $12\% Ni/3\% Zn/Al_2O_3$ catalyst. Once the metals were dissolved in the solvent, a known amount of fumed Al_2O_3 was added to the solution, forming a suspension. The solution was stirred for 5 hours. Water was then removed with a rotavapor and the obtained solid dried overnight in an oven at $120^\circ C$ in air. The dried material was then calcinated at $700^\circ C$ for 2 hours after heating it from room temperature to $700^\circ C$ at a rate of $5.8^\circ C$ /min under an atmosphere of air. The catalyst (prepared and calcinated Ni/Al_2O_3 or $Ni/Zn/Al_2O_3$) was crushed and sieved to a size of 250 micrometers or less. The sieved material was then activated in a tubular quartz reactor placed in a tubular furnace (Lindberg Blue). Nitrogen was flown through the catalyst at a rate of 75mL/min for 30 minutes at room temperature. After that a mixture of hydrogen/nitrogen (35mL/min and 75mL/min, respectively) was flown through the catalyst while it was heated to $700^\circ C$ ($5.8^\circ C/min$) and held at that temperature for 2 hours. The catalyst was then allowed to cool down and was stored in an inert atmosphere for later use.

1.3 Capture Conditions from Pure CO₂

10 mmol of alkali phosphate, for example sodium phosphate (Na_3PO_4) was dissolved in DI water (10 mL) in a vial with a magnetic stir bar, resulting in a one molar solution. The gases inside the vial were then removed under vacuum. CO_2 was subsequently added while stirring the solution at 800 rpm for 3 h and maintaining the CO_2 pressure inside the vessel at 1 psi. The amount of CO_2 captured was calculated both through the volume of CO_2 added and through gravimetric analysis of the solutions before and after the CO_2 capture.

1.4 Hydrogenation Conditions

The catalyst was weighed in an atmosphere of argon and then transported to a nitrogen chamber. There, the capture solution was added to the catalyst. The catalyst and aqueous solution containing the captured CO_2 were placed in a borosilicate vial. This vial was then placed in a 125 mL Hastelloy Parr reactor that was sealed in a nitrogen chamber. The Parr reactor was pressurized with hydrogen (UHP). After that, the reactor was placed in an aluminum block pre-heated to the desired temperature and held at that temperature for the duration of the reaction. At the end of the reaction,

the reactor was cooled to room temperature, the pressure was released, and the solvent was separated from the catalyst via decanting. A portion of the gas mixture was released into a gas collection bag for gas chromatography (GC) analysis.

1.5 Recycling Experiments

Once the hydrogenation reaction according to the method described in 1.4 was complete the reactor was cooled down to room temperature and the pressure released. Part of the pressure was released into a collection bag for gas chromatography analysis. The reactor was then transferred to a nitrogen chamber and opened. The liquid in the reactor was separated from the catalyst by decantation and placed in a 100 mL round bottom flask. This liquid was then subjected to CO_2 capture following the procedure described in 1.3. The amount of CO_2 captured was measured by both the volume of CO_2 added and gravimetrically. The liquid after capture was then placed back in the reactor with the same catalyst that was utilized in the previous cycle. The hydrogenation reaction was then were performed again with the conditions detailed in 1.4.

1.6 Powder X-Ray Diffraction (XRD)

Powder XRD was performed on a sixth generation Rigaku Miniflex powder diffractometer. The catalyst was wet loaded onto a sample plate and then dried of any solvent. The scan was set from 10°-90° at a scan rate of 3°/min. The resulting spectrum were processed on the PDXL software.

1.7 Scanning Electron Microscopy (SEM)

Scanning Electron Microscopy (SEM) images were obtained from a NanoSEM 450 with an accelerating voltage of 10 kV and a spot size of 3 nm.

1.8 X-Ray Fluorescence (XRF)

X-Ray Fluorescence (XRF) was conducted on a Bruker Tiger S8 instrument. The X-Ray source is rhodium leading to residual rhodium signals, which are labelled in the spectra. The spectra were all collected between 0-60 keV. The weight percentages of the metals were calculated using the Bruker software and all errors of the measurements are reported. The calculations were based on the $K\alpha$ peak.

2. Data

2.1 Gas Chromatography Analysis

Gas chromatography was used to analyze the gas mixture and determine if methane and any other gases were produced. Figures S1 and S2 show the gas chromatograms for the reaction that produced 7.1 mmol of CH₄ from 7.1 mmol of captured CO₂ under 50 bar of H₂ at room temperature, 200 °C, 300 mg 5%Ru/Al₂O₃, 10 mL H₂O in 6 hours. The peak at 1.7 minutes is H₂ and is labelled in Figure S1. Methane has a retention time of 4.5 minutes and is labelled in Figure S2. If CO or CO₂ appeared in the spectrum, they would have a retention time of 2.5 and 8.6 minutes, respectively. This shows that the reaction did not produce any gas other than methane. Figures S3 and S4 show the GC data for the reaction conducted at 150 °C. Even at lower temperatures, where not all the captured CO₂ was utilized, no other gas was detected in the gas mixture.

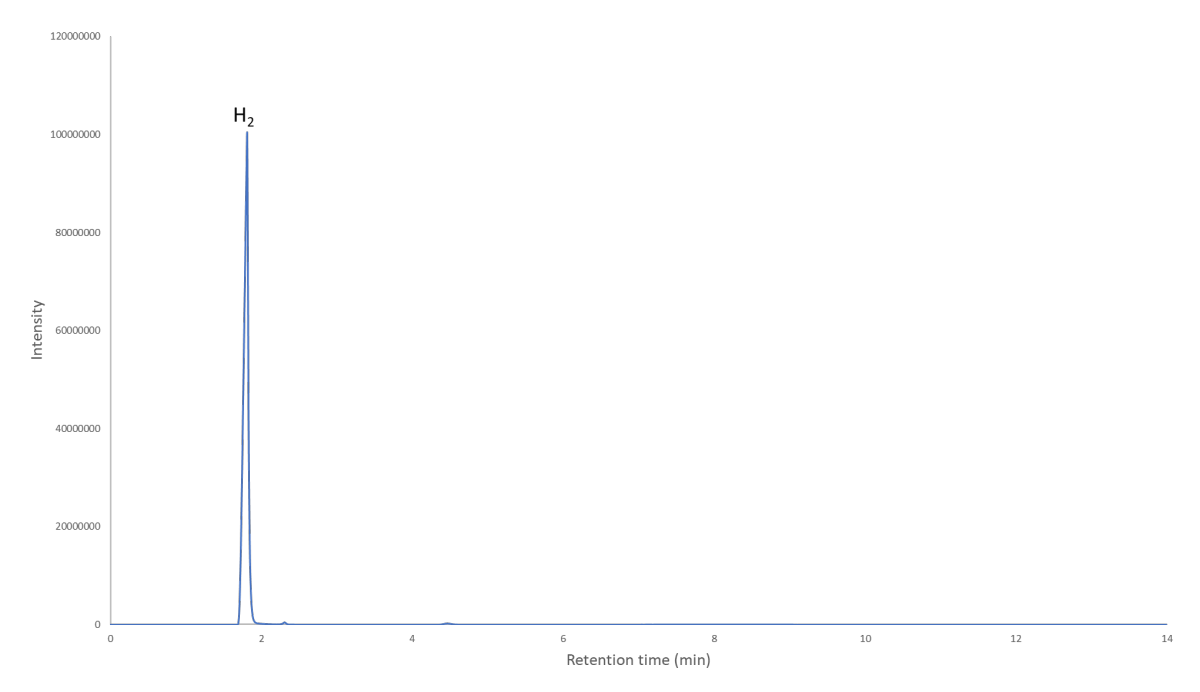


Figure S1. Gas chromatogram of the gas mixture after hydrogenation in a high yielding reaction (conditions: 50 bar H_2 at room temperature, 7.1 mmol of captured CO_2 , 6 hour reaction, 200 °C, 300 mg $5\%Ru/Al_2O_3$, 10 mL H_2O). Peak expansion for methane is shown in Figure S2.

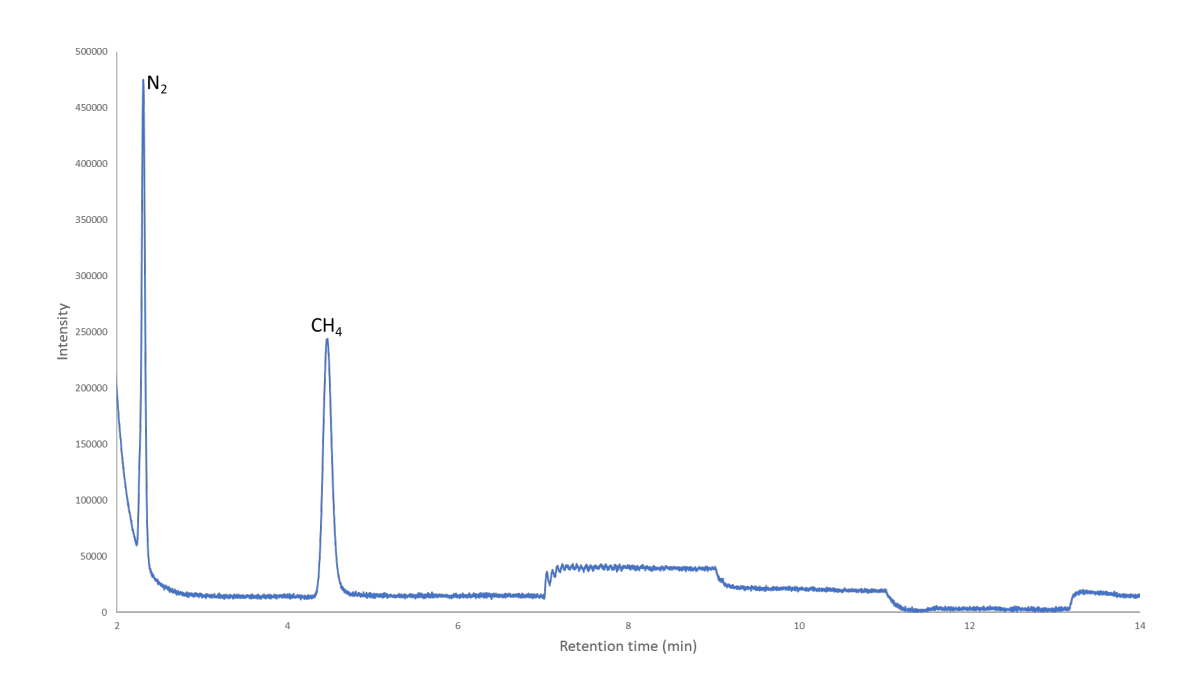


Figure S2. Gas chromatogram of the gas phase after hydrogenation in a high yielding reaction from 2 minutes to 14 minutes (conditions: 50 bar H_2 at room temperature, 7.1 mmol of captured CO_2 , 6 hour reaction, 200 °C, 300 mg 5%Ru/Al₂O₃, 10 mL H_2 O).

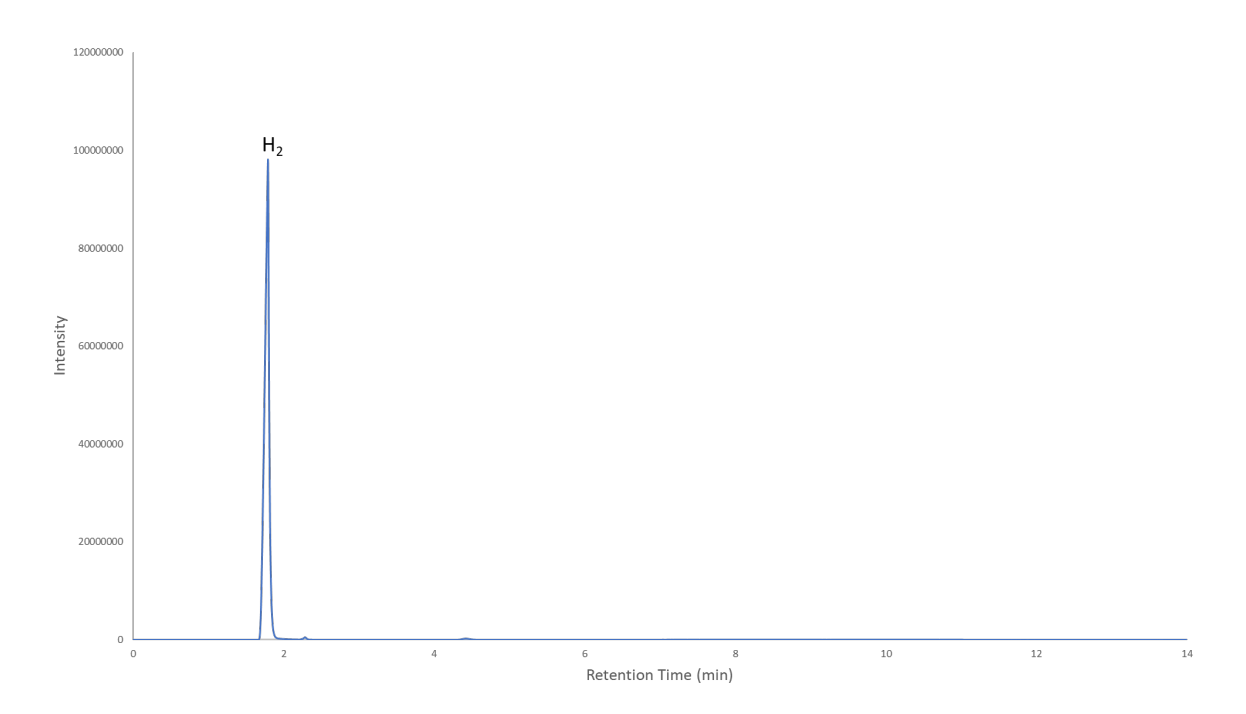


Figure S3. Gas chromatogram of the gas phase after hydrogenation in a reaction at 150 °C (conditions: 50 bar H_2 at room temperature, 7.1 mmol of captured CO_2 , 6 hours, 150 °C, 300 mg 5%Ru/Al₂O₃, 10 mL H_2O). Peak expansion for methane is shown in Figure S4.

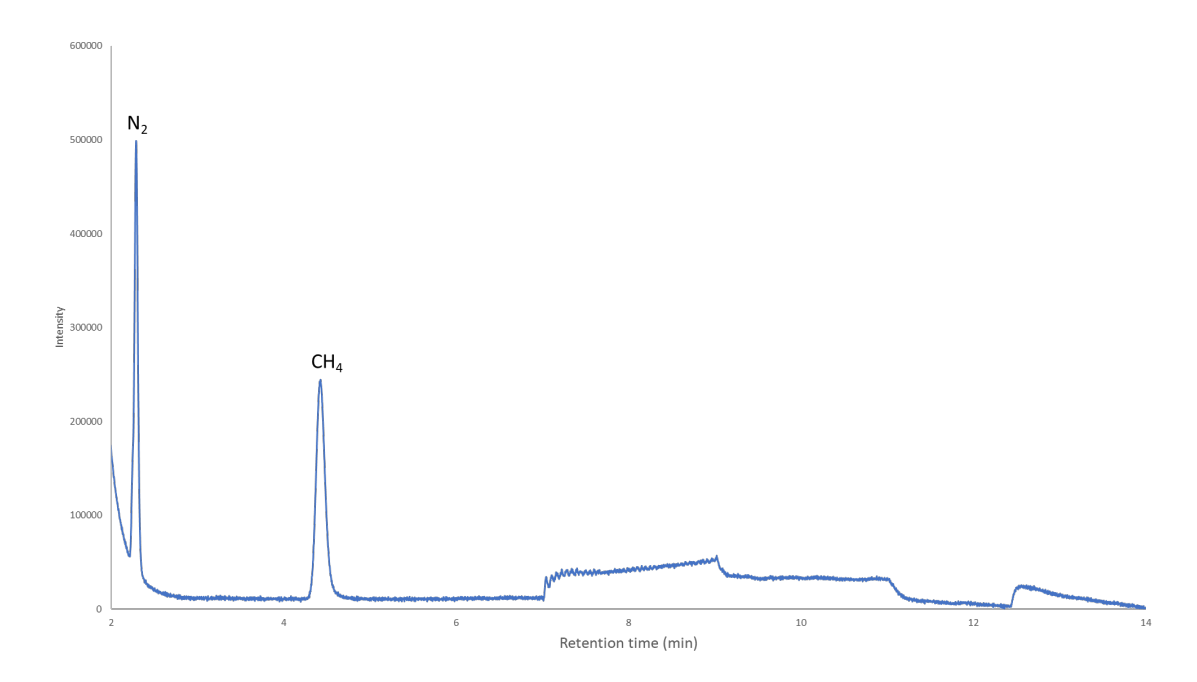


Figure S4. Gas Chromatogram of the gas phase after hydrogenation in a reaction at 150 °C from 2 minutes to 14 minutes (conditions: 50 bar H_2 at room temperature, 7.1 mmol of captured CO_2 , 6 hours, 150 °C, 300 mg 5%Ru/Al₂O₃, 10 mL H_2 O).

To calculate the amount of methane that was produced, the integration values were obtained from the gas chromatogram. For example, the chromatograms shown in figures S1 and S2 have $99.26\%~H_2$ and $0.74\%~CH_4$. Nitrogen is excluded from the calculation (it is due to air present during the injection using a gas syringe). These integration values are normalized to account for their response factors. Once the response factors are accounted for the integration values are $97.21\%~H_2$ and $2.79\%~CH_4$. The pressure prior to releasing the gas was recorded and utilized for the next step of the calculation. The pressure of 710 psi at the time of release is multiplied by the percentage of methane. This results in 19.81 psi of methane. This is converted to atm for further computations by dividing the pressure in psi by 14.696 to obtain pressure in atm; in this case 1.347 atm. This pressure is then used in gas law's equation to compute the amount of moles of methane as shown in equation S1. The temperature that is used for the calculation is the temperature at the time of the release of the gas. After using gas law's equation, there was 7.1 mmol of methane in the gas released from the reactor, which corresponds to the 100% yield we observed.

$$mol \ of \ methane = \frac{(1.347 \ atm)(0.130 \ L)}{(27.0 \ ^{\circ}\text{C} + 273.15)(0.0821 \ \frac{atm * L}{mol * K})}$$

Equation S1. Example calculation showing the amount of methane (mol) produced, where the volume is the volume of the reactor was 0.130 L, the temperature is the temperature at which the gas is released, and R is the ideal gas constant.

2.2 NMR Data

Nuclear Magnetic Resonance (NMR) data was also collected to test how the phosphate salt was capturing the carbon dioxide. Figure S5 shows the ³¹PNMR of sodium phosphate tribasic, Na₃PO₄, referenced to a triphenylphosphine oxide standard, which shows a peak at 5.51 ppm. Figure S6 shows the ³¹P NMR of sodium phosphate dibasic, Na₂HPO₄, referenced to triphenylphosphine oxide with a peak at 3.28 ppm. Figure S8 shows the ³¹P NMR (referenced to triphenylphosphine oxide) of the capture solution after being subjected to the carbon dioxide capture conditions described in 1.3 of the SI. The peak in Figure S6, at 4.03 ppm, is further up-field from the peak shown in Figure S5, which is consistent with the phosphate salt becoming protonated. However, it is not fully the sodium phosphate dibasic peak. This indicates that the phosphate salt is deprotonating the water and that the resulting hydroxide anion is assisting in the capture. This is further shown in Figure S9, which is the ¹³C NMR of the capture solution referenced to the internal imidazole standard (121.9 ppm). This shows a peak at 161, which is similar to sodium bicarbonate, NaHCO₃. However, upon increasing the capture time from 3 hours to 12 hours the peak in ³¹P NMR shifts further up-field and is similar to the sodium phosphate dibasic peak and shows at 3.28 ppm as shown in Figure S8.

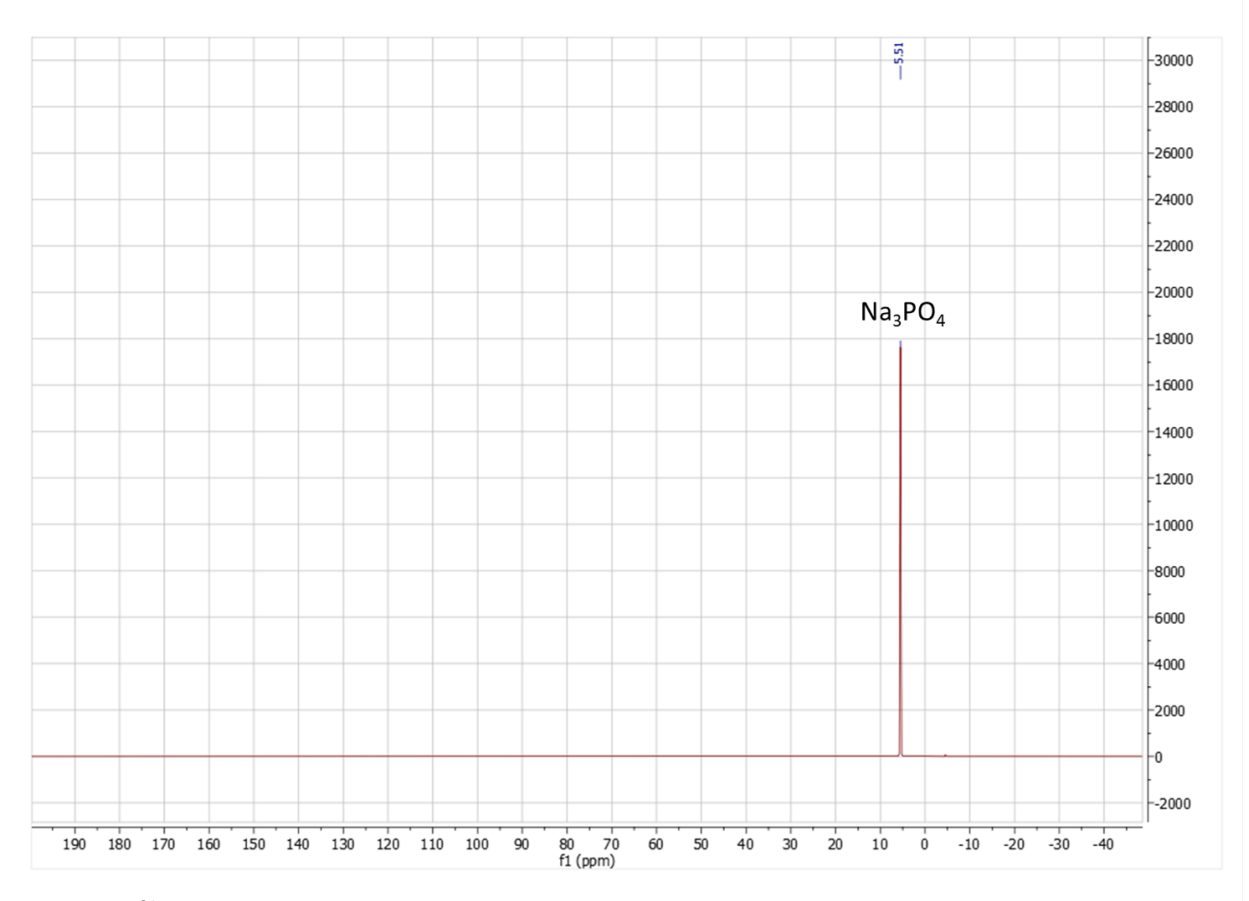


Figure S5. 31P NMR of sodium phosphate tribasic, Na₃PO₄.

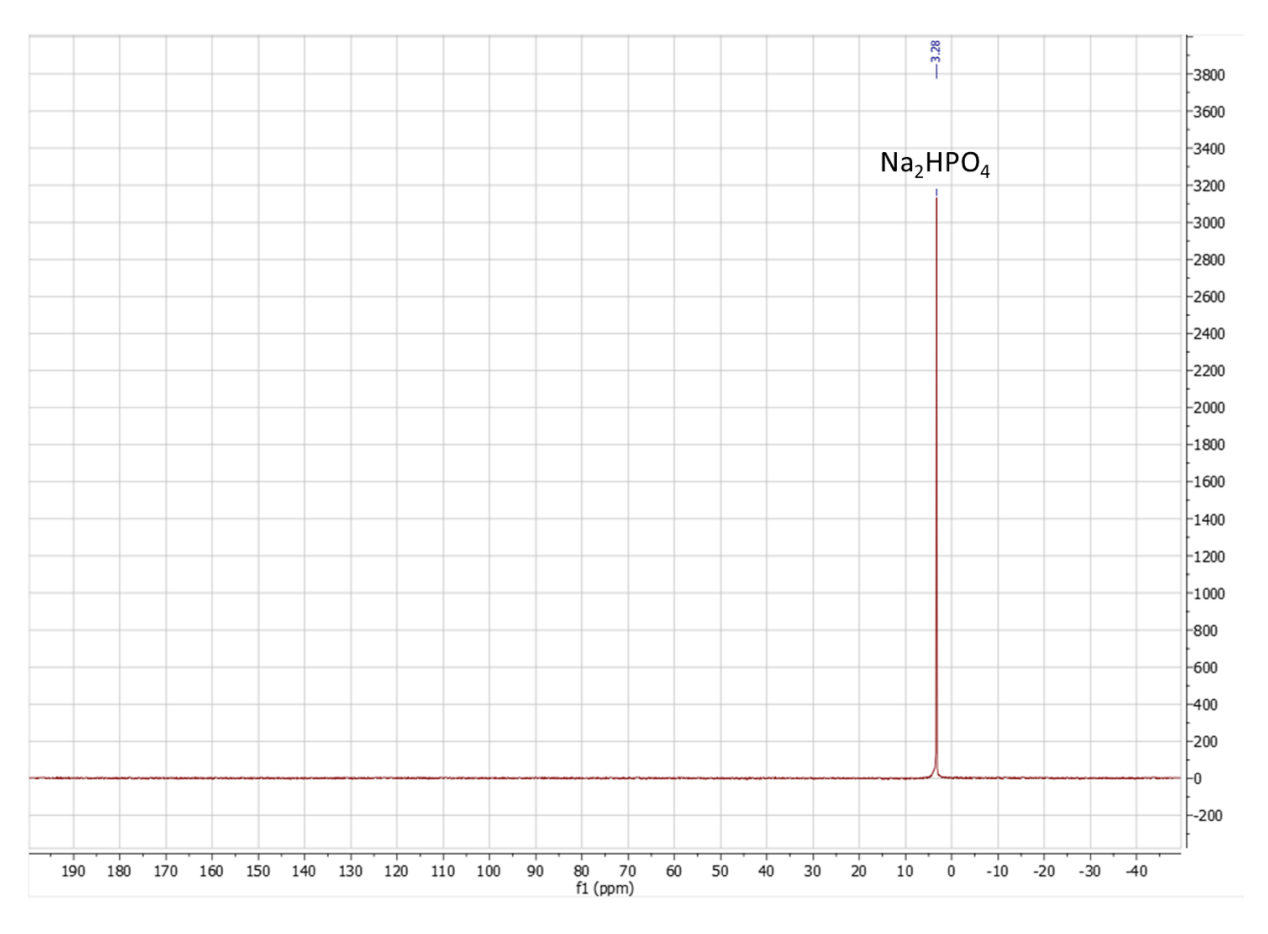


Figure S6. ³¹P NMR of sodium phosphate dibasic, Na₂HPO₄.

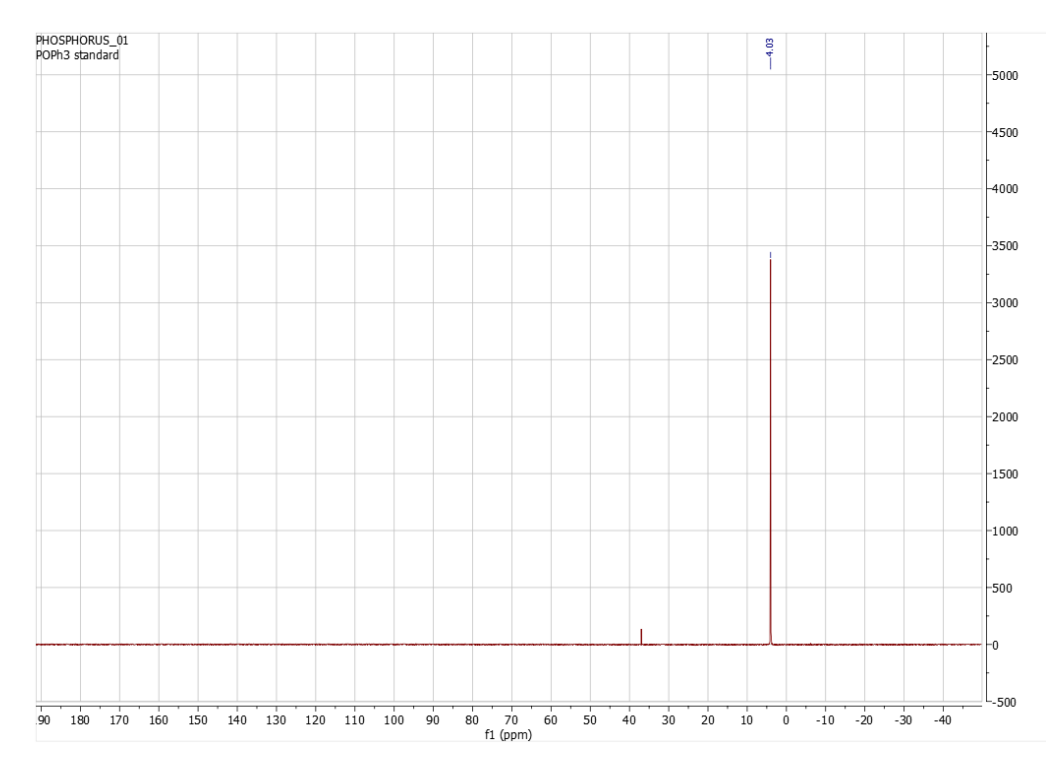


Figure S7. ^{31}P NMR of the sodium phosphate tribasic capture solution after 3-hour CO $_2$ capture.

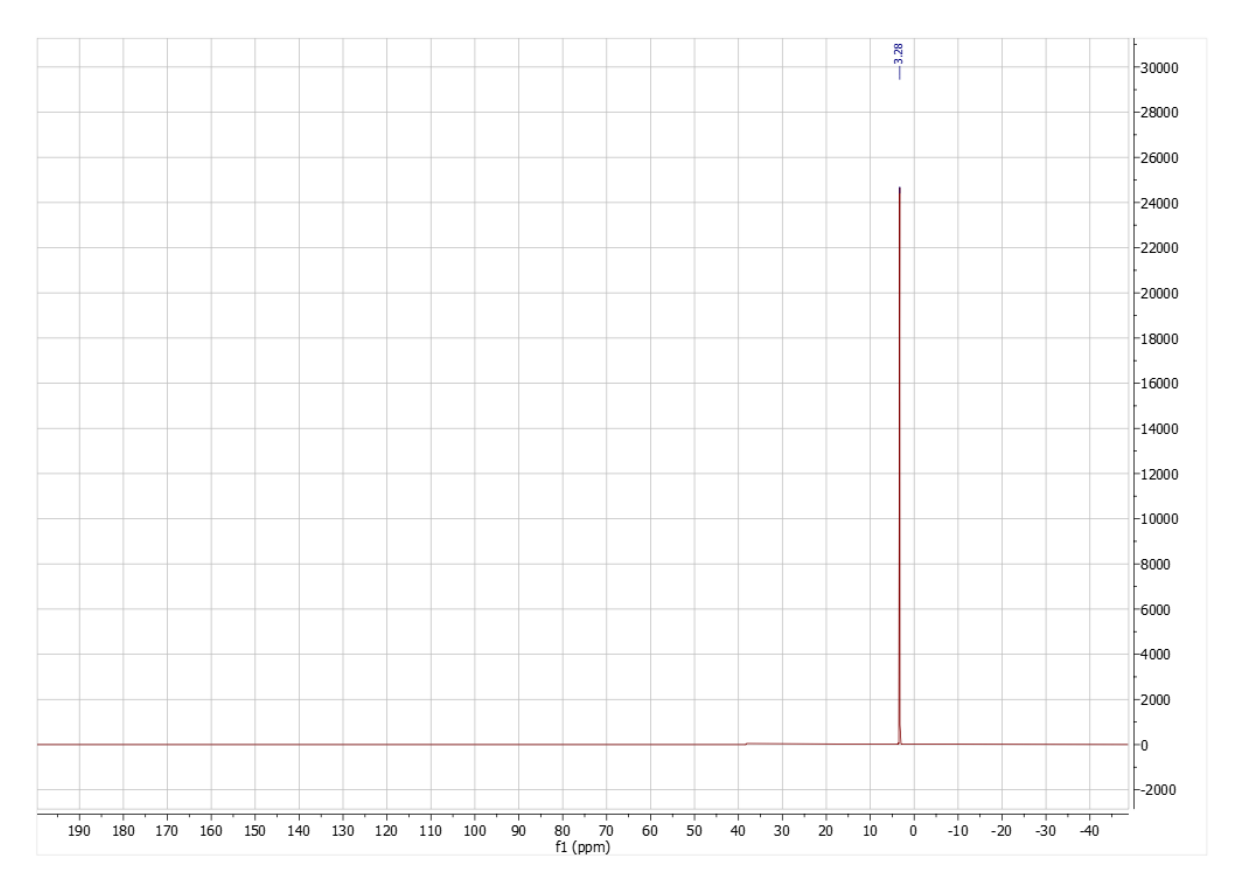


Figure S8. ^{31}P NMR of the sodium phosphate tribasic capture solution after 12-hour CO $_{2}$ capture.

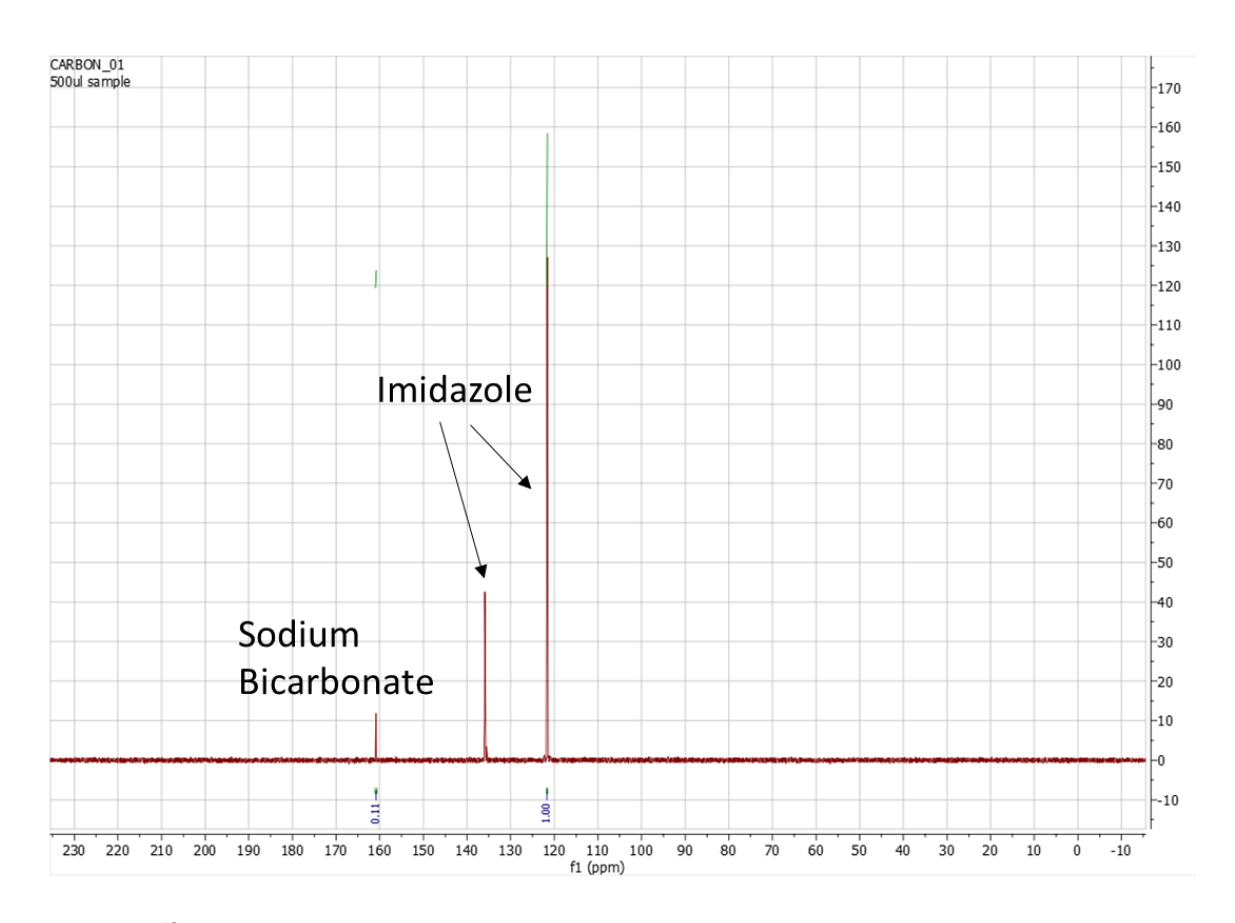


Figure S9. ¹³C NMR of the sodium phosphate tribasic capture solution after CO₂ capture.

Figure S10 shows the ³¹P NMR of the reaction mixture after reaction with 5%Ru/Al₂O₃. It is evident that we still have a phosphate peak, at 4.27 ppm. This peak is located between the one for sodium phosphate tribasic (5.51 ppm, Figure S5) and sodium phosphate dibasic (3.28 ppm, Figure S6), which could mean that a mixture of these two sodium phosphate is be present after the reaction. This also shows that after the first reaction there is phosphate regeneration. However, upon looking at the ³¹P NMR of the reaction mixture after five cycles of reaction, the peak is at 2.36 ppm as shown in Figure S11, which is upfield of the peak for sodium phosphate dibasic. This peak is most likely the result of a mixture of sodium phosphate dibasic and monobasic. There are no other peaks besides the peak at 2.36 ppm and the triphenylphosphine oxide reference. This means that the phosphate salt is becoming less basic over consecutive cycles and explains why the recycling experiments are not quantitative over longer lengths of reaction time as the solution is no longer basic enough to efficiently capture CO₂.

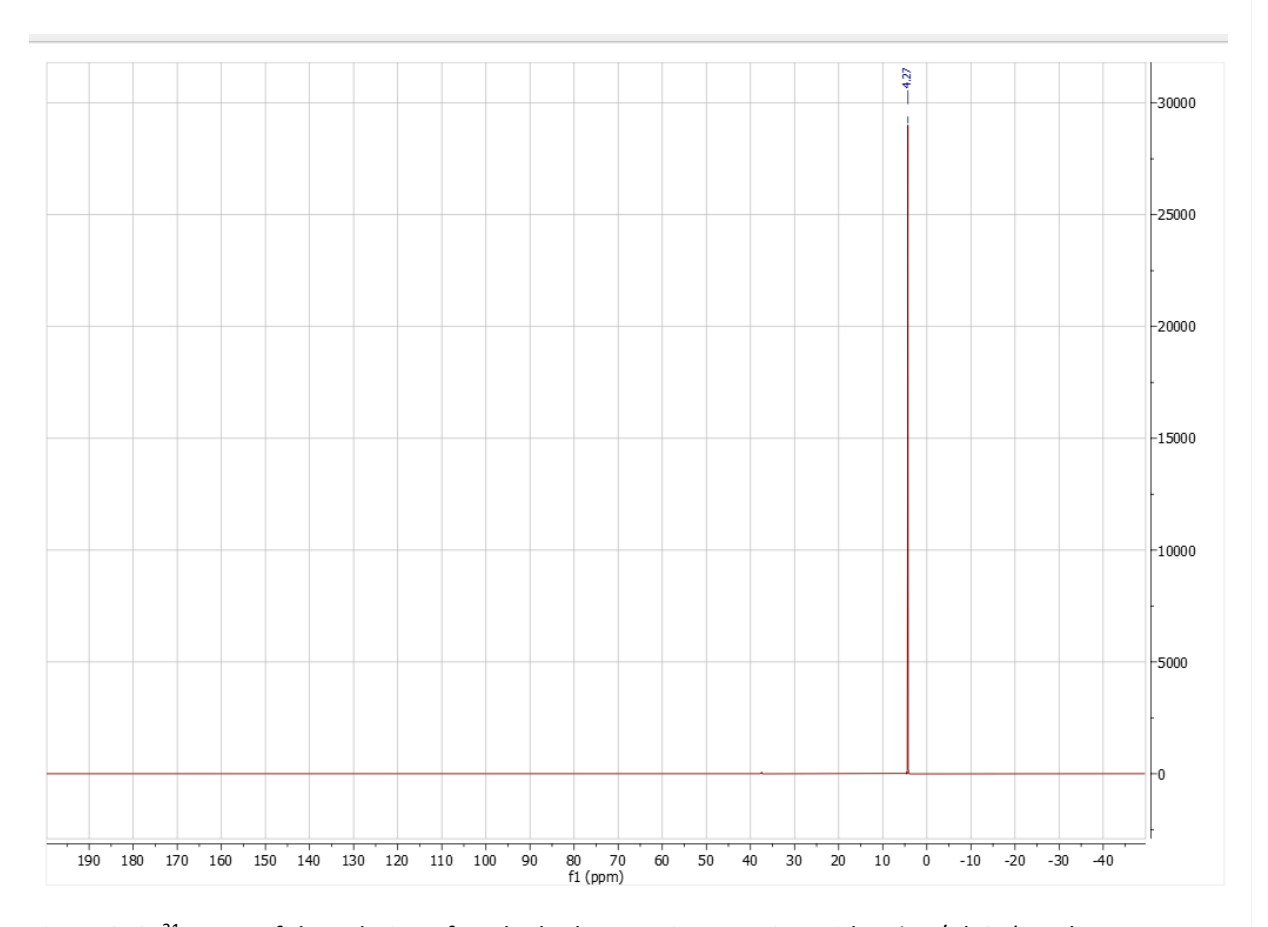


Figure S10. 31 PNMR of the solution after the hydrogenation reaction with 5%Ru/Al₂O₃ (conditions: 300mg $^{5\%}$ Ru/Al₂O₃, 11.3 mmol captured CO₂, 200 °C, 6 hours, 60 bar H₂).

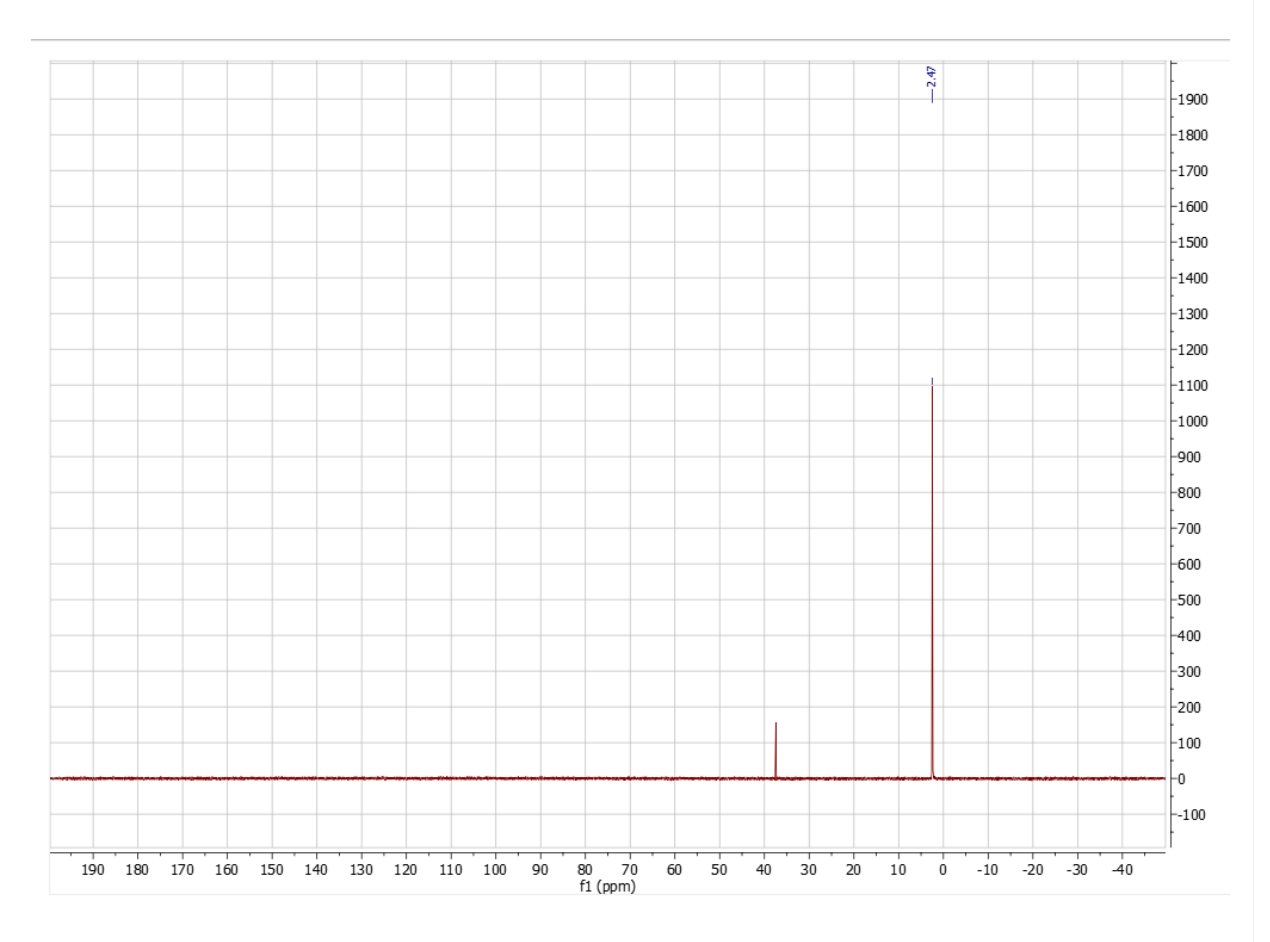


Figure S11. ^{31}P NMR of the solution after 5 cycles of reactivity with the $5\%Ru/Al_2O_3$ catalyst.

 1 H NMR of the gas mixture after the hydrogenation reaction over 5%Ru/Al $_{2}$ O $_{3}$ was also taken to check if any other gases beside H $_{2}$ and methane were present at the end of the reaction. Figure S12 displays the 1 HNMR of the gas mixture after reaction, which shows that beside hydrogen and methane no other gaseous products were present.

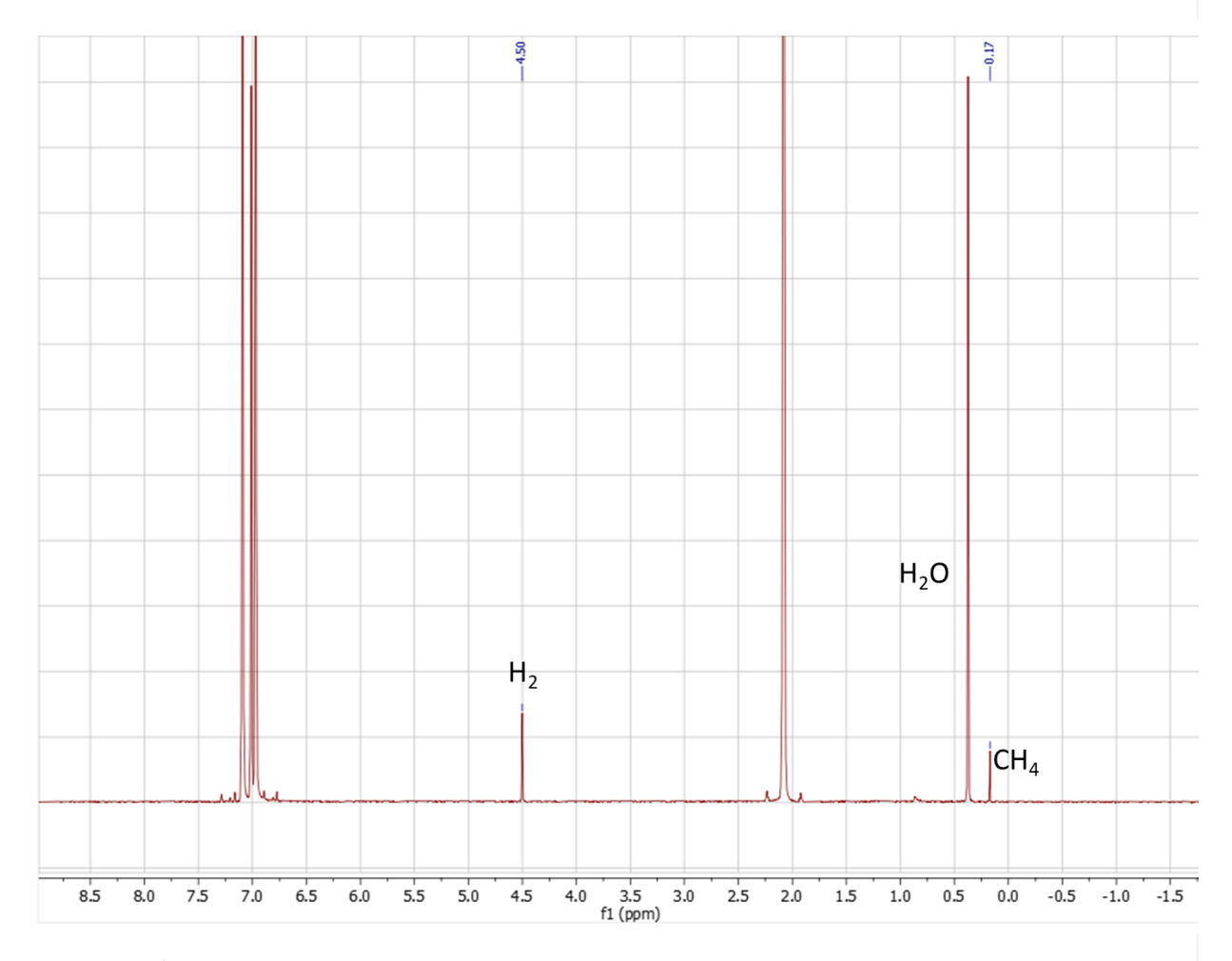


Figure S12. 1 H NMR of gas mixture after the hydrogenation reaction with 5%Ru/Al₂O₃ (conditions: $_{300mg}$ $_{5\%$ Ru/Al₂O₃, $_{11.3}$ mmol captured CO₂, $_{200}$ °C, $_{60}$ hours, $_{60}$ bar H₂).

2.3 X-Ray Diffraction Data

X-Ray Diffraction (XRD) spectra were taken for each catalyst before and after reaction with the capture solution. D-spacing calculations for each catalyst for the primary metal are shown in table S1 and were calculated with Bragg's law.

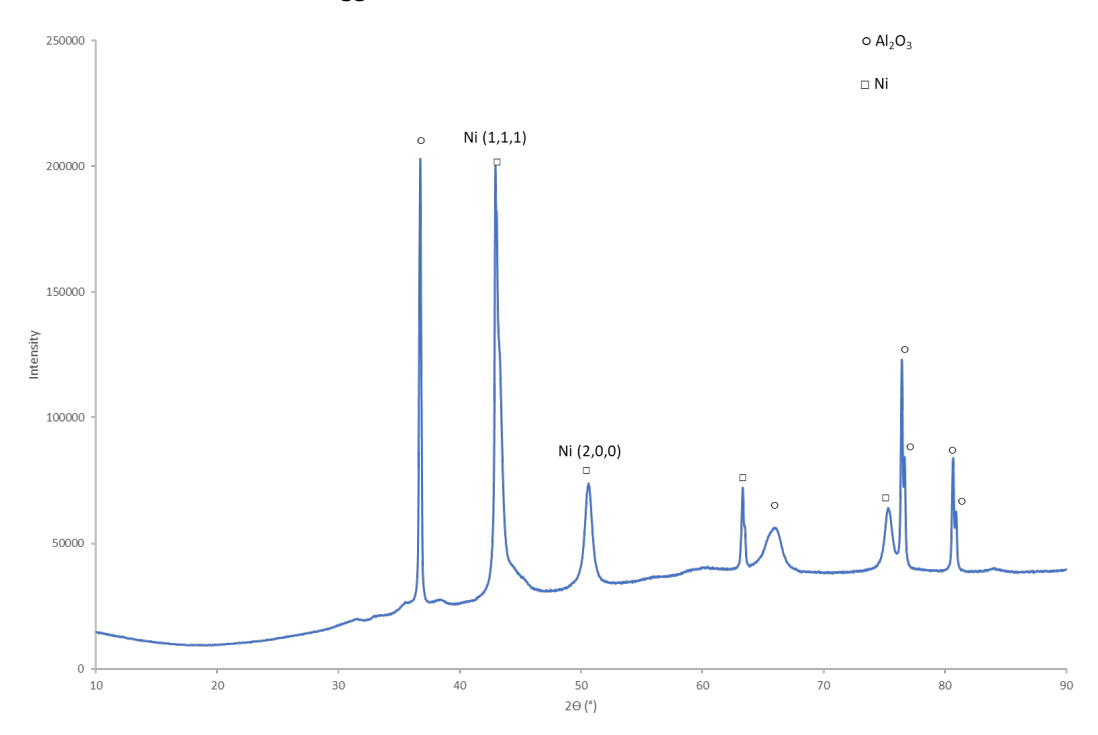


Figure S13. XRD of 25%Ni/Al₂O₃ before reaction.

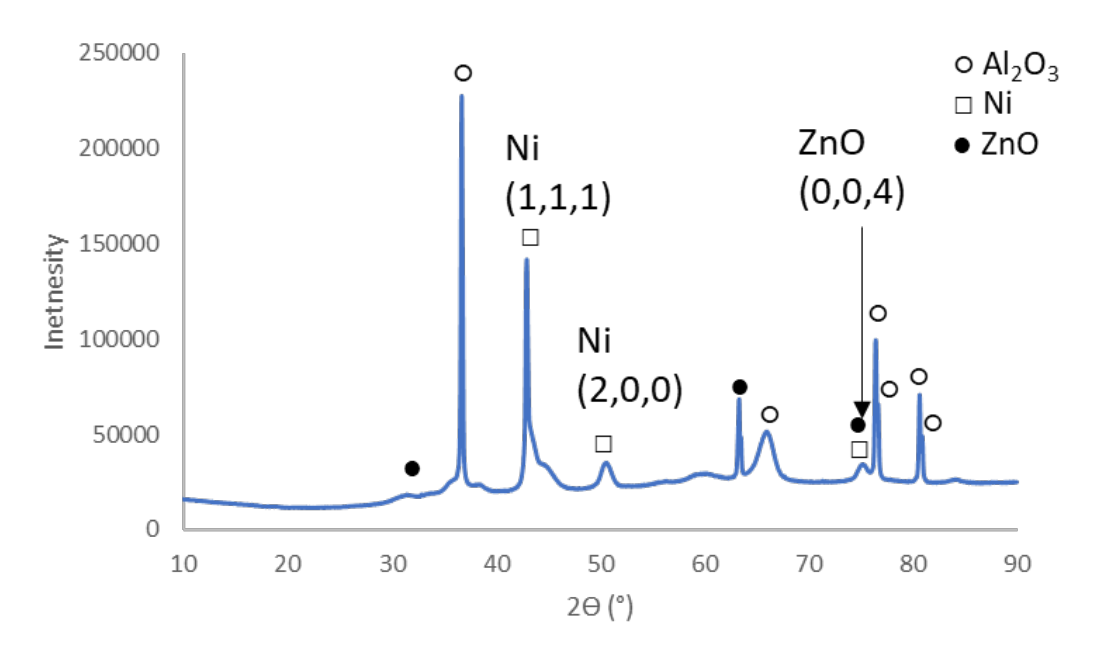


Figure S14. XRD of 12%Ni/3%Zn/Al₂O₃ before reaction.

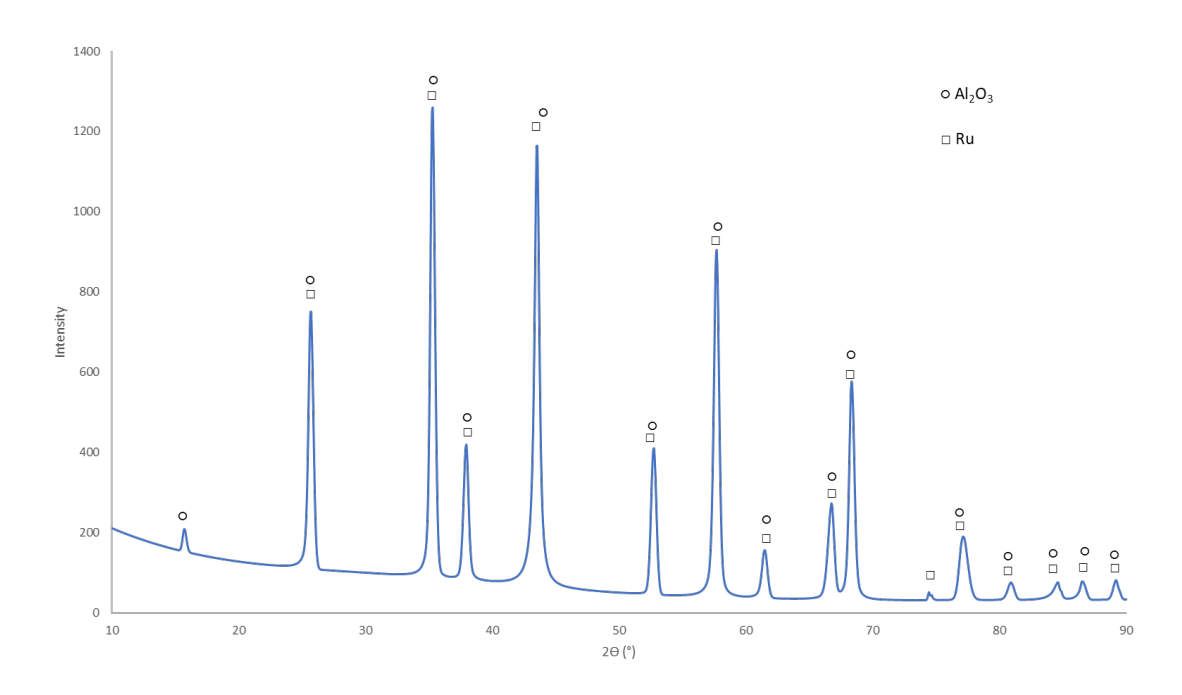


Figure S15. XRD of 5%Ru /Al₂O₃ before reaction.

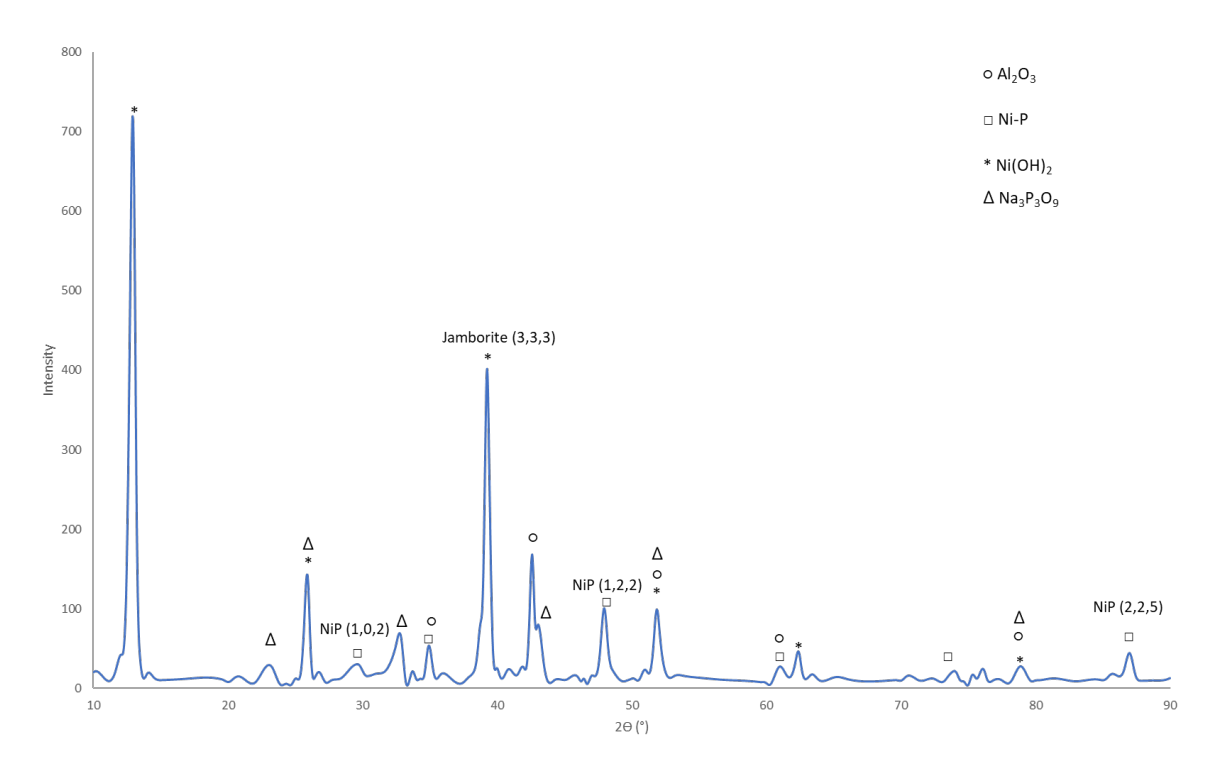


Figure S16. XRD of 25%Ni/Al $_2$ O $_3$ after the hydrogenation reaction of the aqueous Na $_3$ PO $_4$ capture solution.

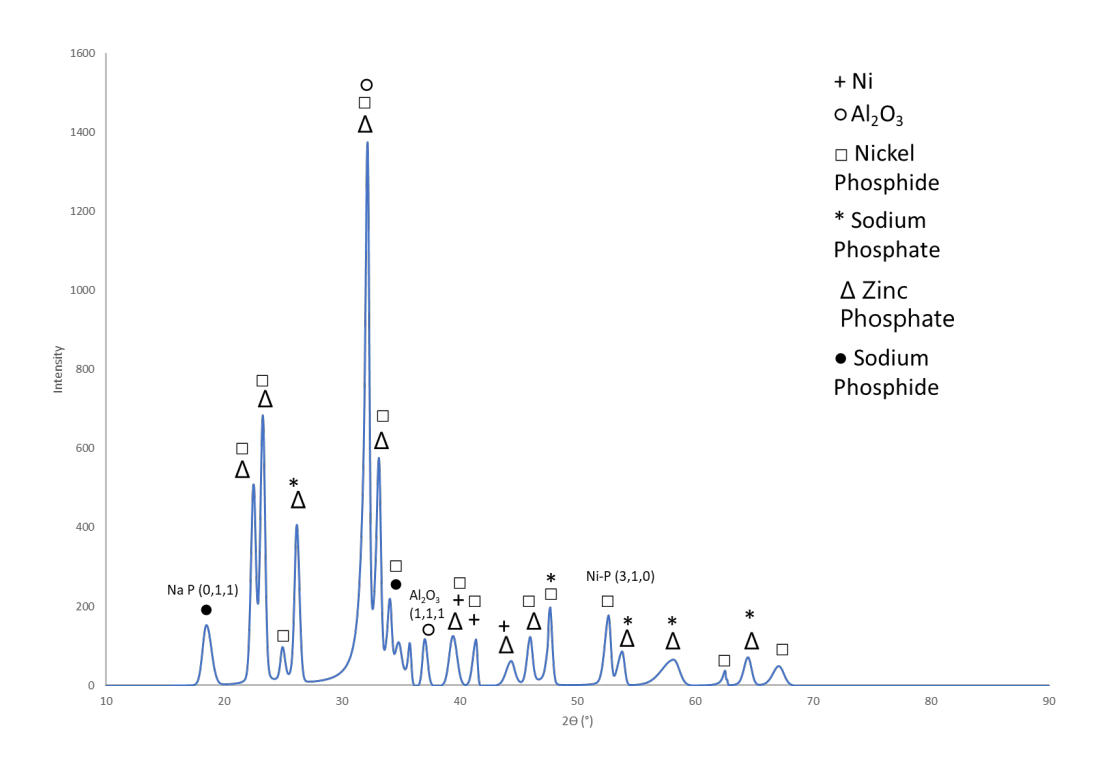


Figure S17. XRD of 12%Ni/3%Zn/Al $_2$ O $_3$ after the hydrogenation reaction with the aqueous Na $_3$ PO $_4$ capture solution.

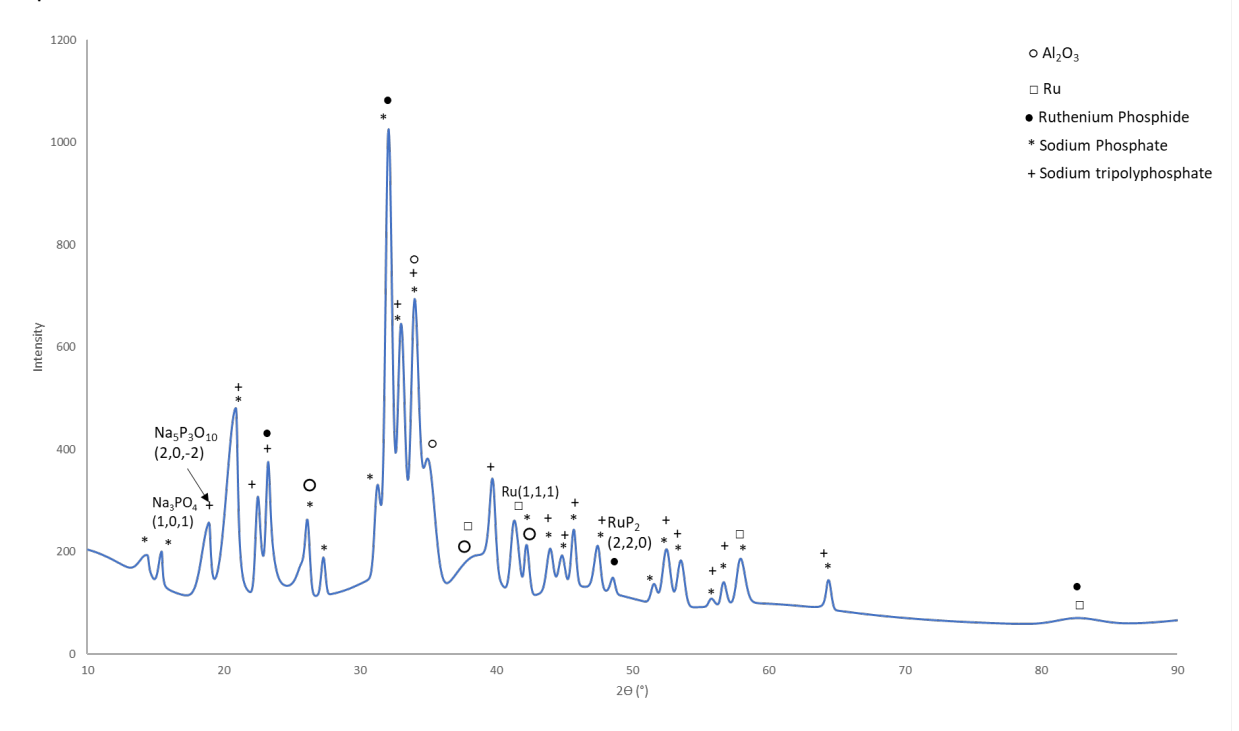


Figure S18. XRD of 5%Ru/Al₂O₃ after the hydrogenation reaction with the aqueous Na₃PO₄ capture solution.

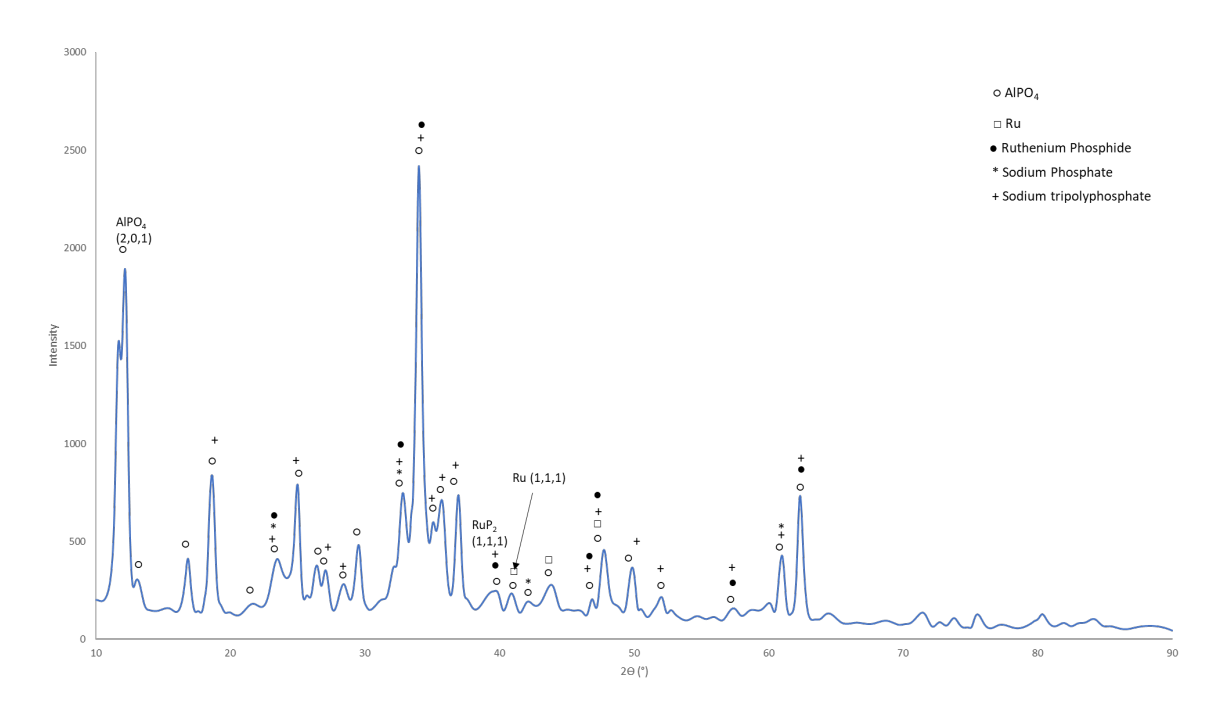


Figure S19. XRD of 5%Ru/Al₂O₃ and other solid materials after 5 cycles of hydrogenation reaction with the Na₃PO₄ capture solution.

Table S1. Table of XRD Data

Catalyst	Peak chosen	d-spacing (Å)	Crystallite Size (Å)
25%Ni/Al ₂ O ₃	Ni (1,1,1)	2.0931 (5)	144 (3)
12%Ni/3%Zn/Al ₂ O ₃	Ni (1,1,1)	2.0880 (6)	44.2 (5)
5%Ru/Al ₂ O ₃	Ru (1,1,1)	2.0787 (17)	217 (18)
25%Ni/Al ₂ O ₃ after reaction	Ni (1,1,1)	2.10248 (9)	225 (41)
12%Ni/3%Zn/Al ₂ O ₃ after reaction	Ni (1,1,1)	2.12616 (8)	177 (12)
5%Ru/Al₂O₃ after reaction	Ru (1,1,1)	2.0603 (18)	134 (9)
5%Ru/Al ₂ O ₃ after 5 cycles of reaction	Ru(1,1,1)	2.2040 (15)	224 (31)

d-space is calculated with Bragg's law, all calculation errors are shown in parentheses, error is \pm the number in parentheses referenced to the last digit

2.4 SEM Images

SEM images were collected of the 5%Ru/Al₂O₃ catalyst before and after the reaction with conditions 10 mmol Na₃PO₄ salt after 3 hours under pure CO₂ stream, 10 mL DI H₂O, 200 °C, 6 hours reaction time, 300 mg 5%Ru/Al₂O₃, 50 bar H₂ and are shown in Figures S14 and S15 respectively.

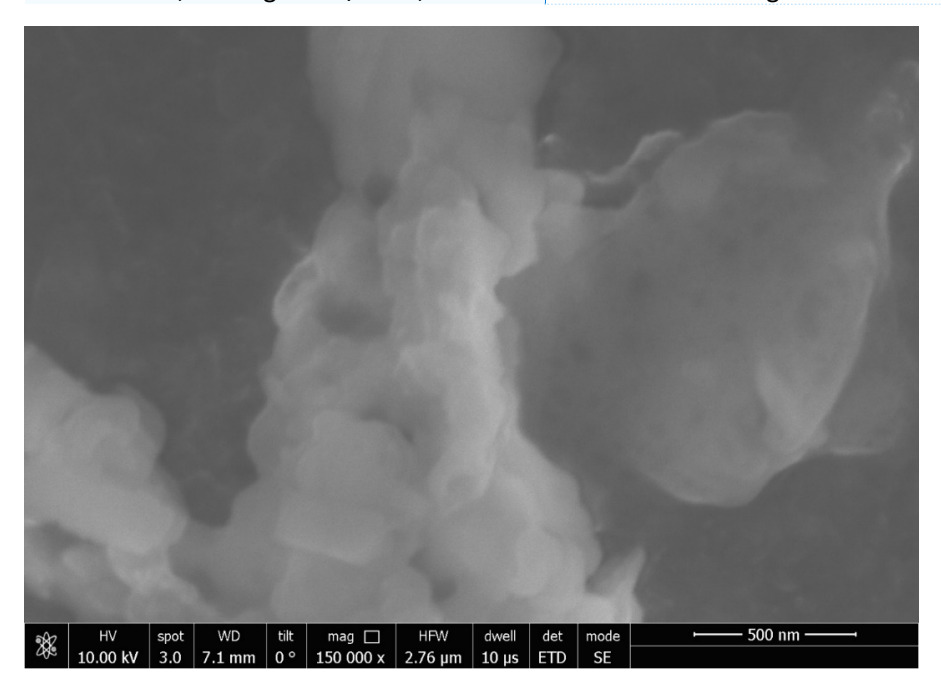


Figure S20. SEM image of $5\%Ru/Al_2O_3$ before the reaction.

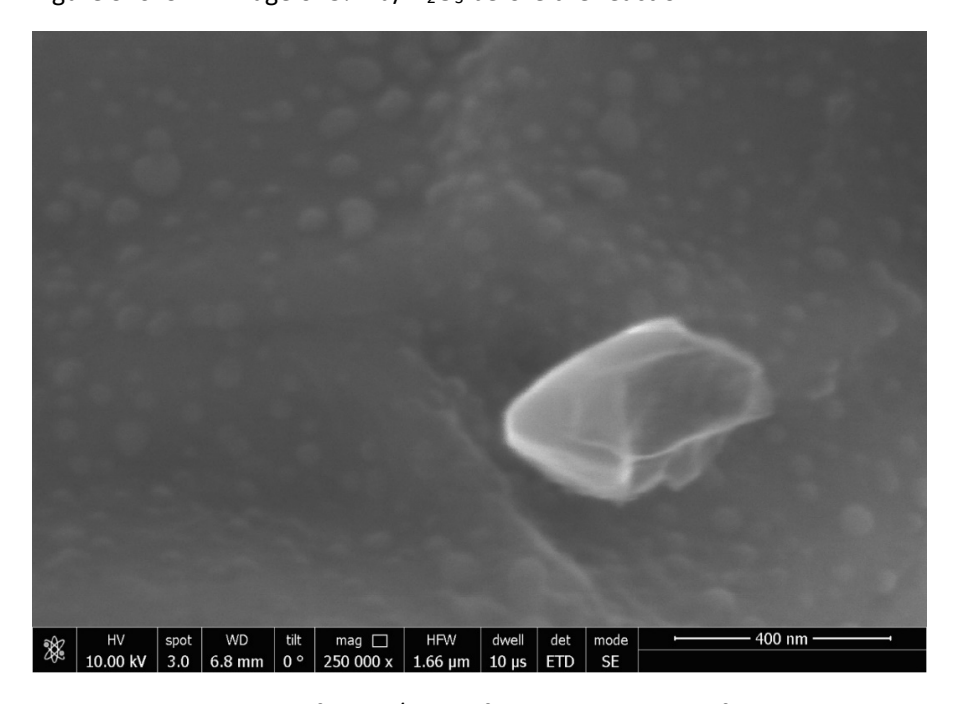


Figure S21. SEM image of 5%Ru/Al₂O₃ after hydrogenation of the Na₃PO₄ capture solution.

2.5 X-Ray Fluorescence Data (XRF)

XRF measurements were obtained to calculate the weight concentrations of each metal on the catalysts. All measurements are shown with errors. The radiation is detected by three types of crystals (LiF200, XS-55, and PET), which required each spectrum to have several runs so that each crystal can be used for detection. This results in what looks like different baselines that can often be seen above 20 KeV.

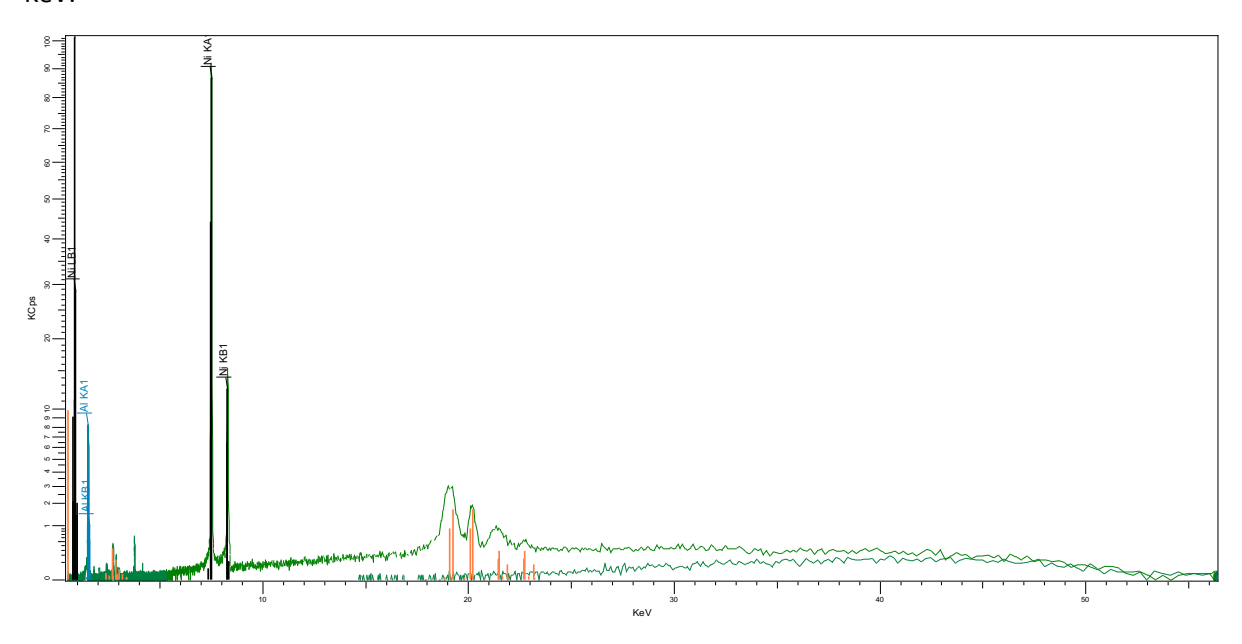


Figure S22. XRF spectra of 25%Ni/Al₂O₃

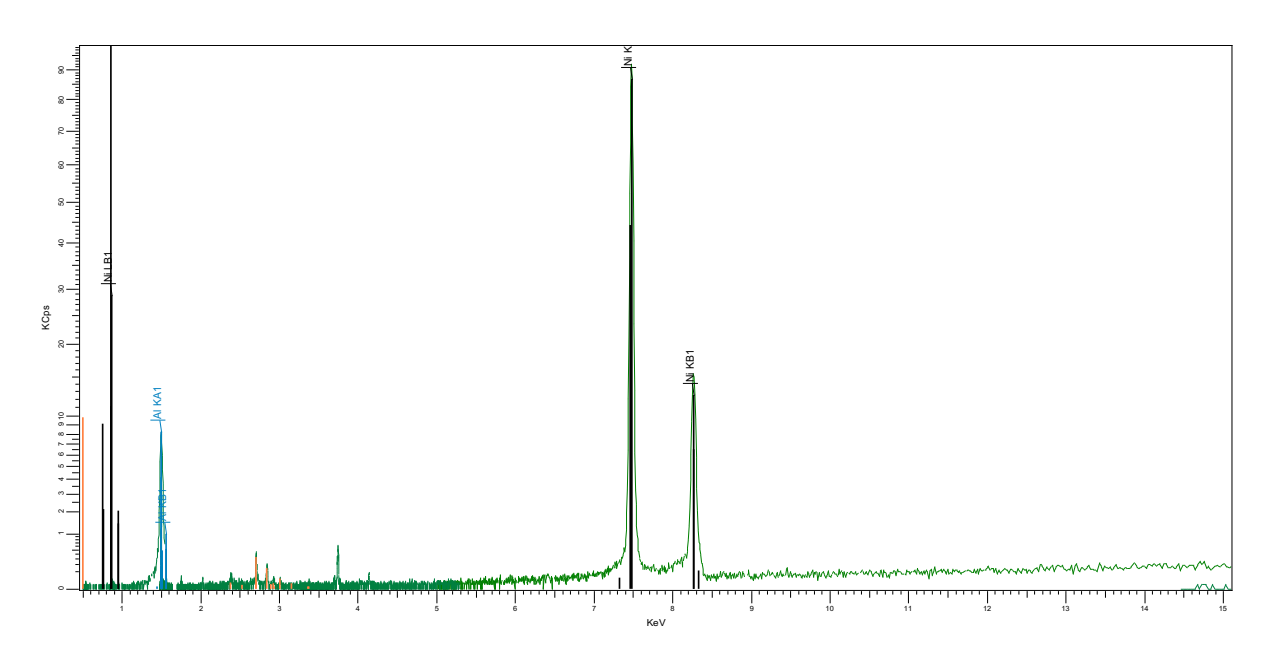


Figure S23. XRF spectra of 25%Ni/Al $_2$ O $_3$ zoomed into 0-15KeV

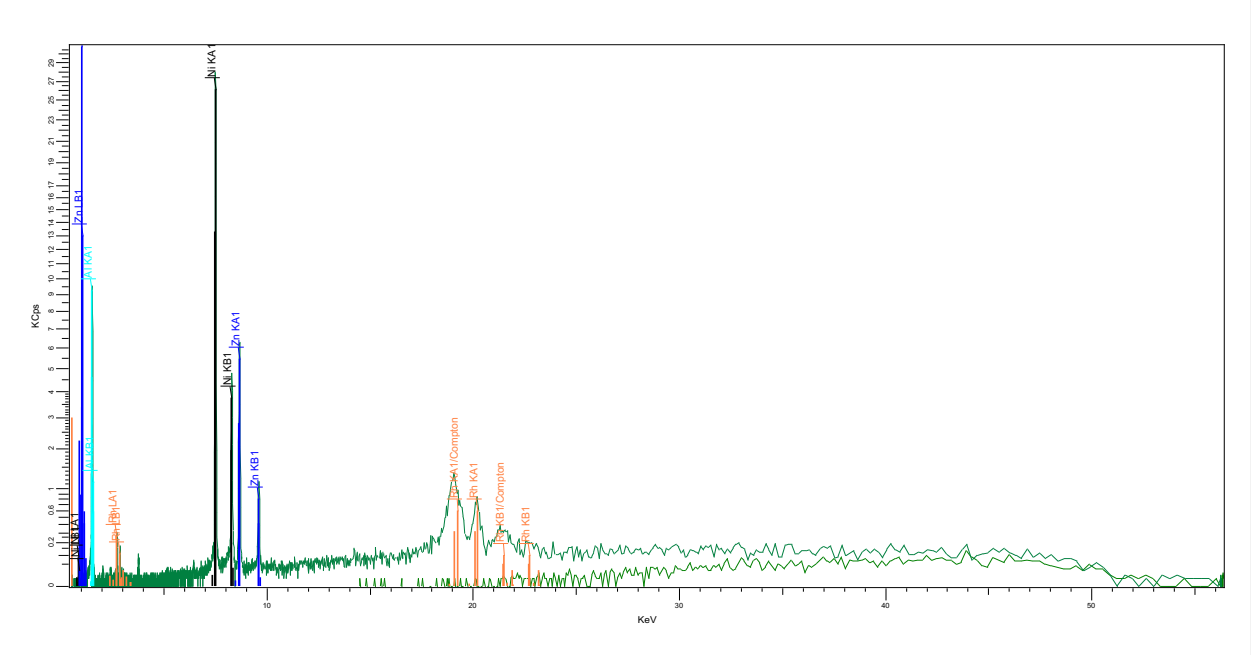


Figure S24. XRF spectra of 12%Ni/3%Zn/Al₂O₃

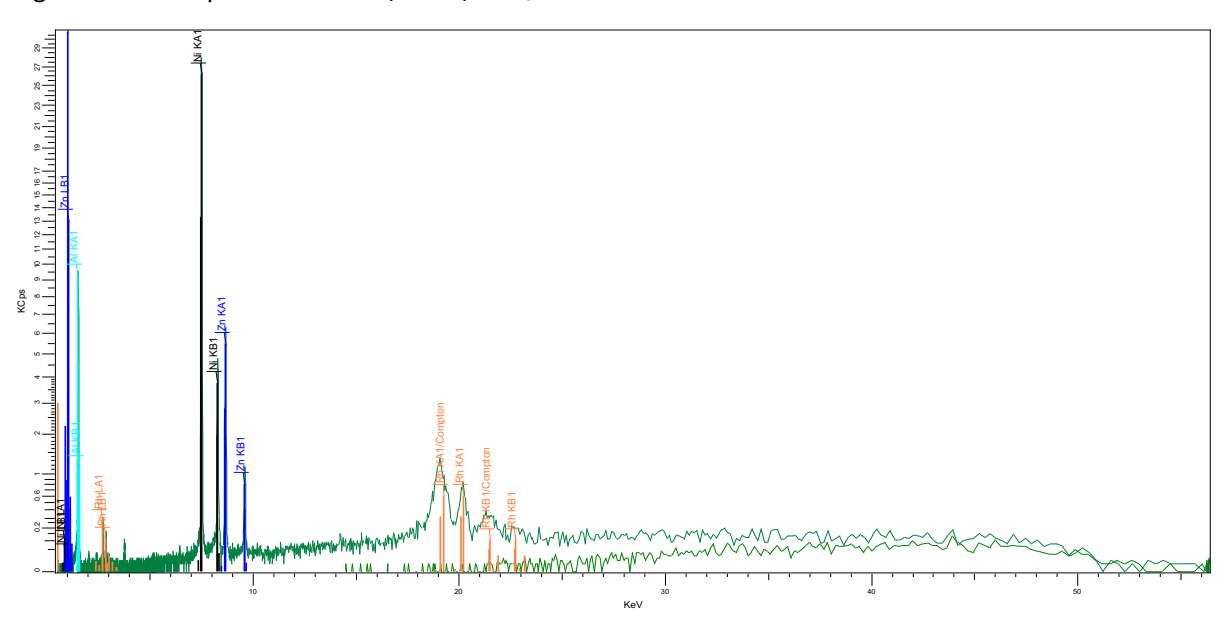


Figure S25. XRF spectra of $12\%Ni/3\%Zn/Al_2O_3$ zoomed between 0-11 KeV

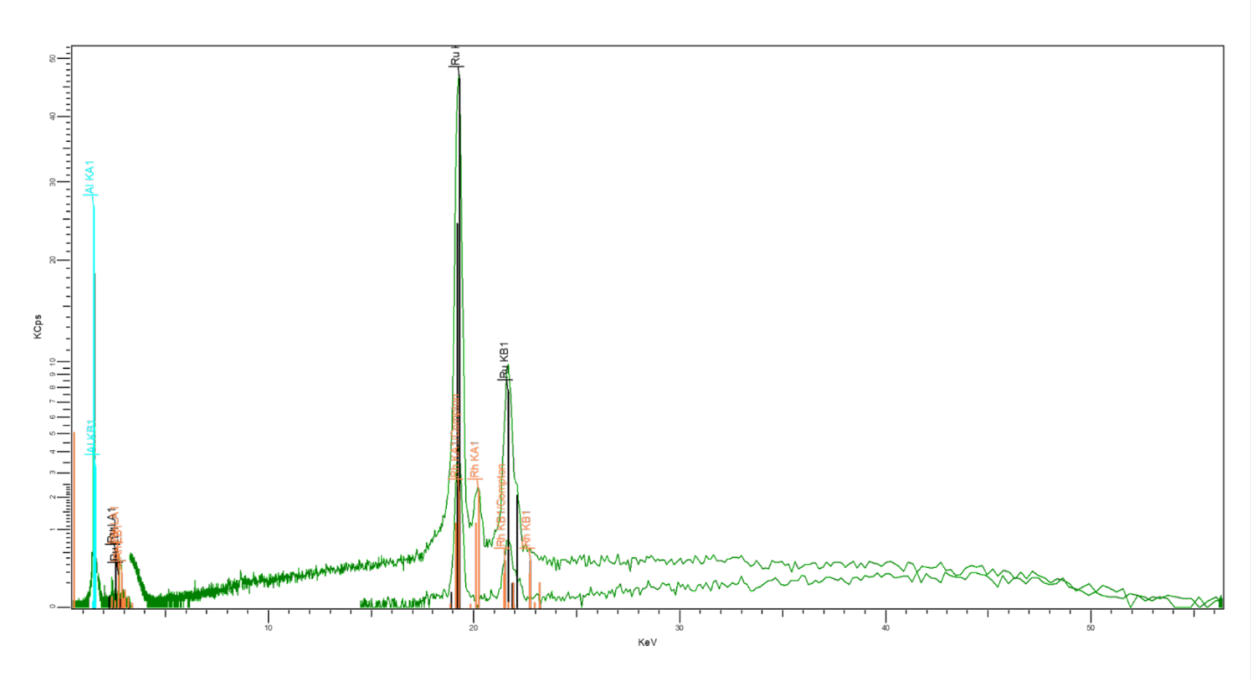


Figure S26. XRF of commercial 5%Ru/Al₂O₃

Table S2. Weight percentages of synthesized catalysts

Catalyst	Nickel (%w)	Zinc (%w)
25%Ni/Al ₂ O ₃	25.80±0.35	N/A
12%Ni/3%Zn/Al ₂ O ₃	11.94±0.62	2.28±1.33
5%Ru/Al ₂ O ₃	6.27±1.62	N/A